

Apoptosis reprogramming triggered by splicing inhibitors sensitizes multiple myeloma cells to Venetoclax treatment

by Debora Soncini, Claudia Martinuzzi, Pamela Becherini, Elisa Gelli, Samantha Ruberti, Katia Todoerti, Luca Mastracci, Paola Contini, Antonia Cagnetta, Antonella Laudisi, Fabio Guolo, Paola Minetto, Maurizio Miglino, Sara Aquino, Riccardo Varaldo, Daniele Reverberi, Matteo Formica, Mario Passalacqua, Alessio Nencioni, Antonino Neri, Mehmet K. Samur, Nikhil C. Munshi, Mariateresa Fulciniti, Roberto M. Lemoli, and Michele Cea

Received: September 2, 2021.

Accepted: October 13, 2021.

Citation: Debora Soncini, Claudia Martinuzzi, Pamela Becherini, Elisa Gelli, Samantha Ruberti, Katia Todoerti, Luca Mastracci, Paola Contini, Antonia Cagnetta, Antonella Laudisi, Fabio Guolo, Paola Minetto, Maurizio Miglino, Sara Aquino, Riccardo Varaldo, Daniele Reverberi, Matteo Formica, Mario Passalacqua, Alessio Nencioni, Antonino Neri, Mehmet K. Samur, Nikhil C. Munshi, Mariateresa Fulciniti, Roberto M. Lemoli, and Michele Cea. Apoptosis reprogramming triggered by splicing inhibitors sensitizes multiple myeloma cells to Venetoclax treatment.

Haematologica. 2021 Oct 21. doi: 10.3324/haematol.2021.279276. [Epub ahead of print]

Publisher's Disclaimer.

E-publishing ahead of print is increasingly important for the rapid dissemination of science. Haematologica is, therefore, E-publishing PDF files of an early version of manuscripts that have completed a regular peer review and have been accepted for publication. E-publishing of this PDF file has been approved by the authors. After having E-published Ahead of Print, manuscripts will then undergo technical and English editing, typesetting, proof correction and be presented for the authors' final approval; the final version of the manuscript will then appear in a regular issue of the journal. All legal disclaimers that apply to the journal also pertain to this production process.

Apoptosis reprogramming triggered by splicing inhibitors sensitizes multiple myeloma cells to Venetoclax treatment

Debora Soncini¹, Claudia Martinuzzi^{1,2}, Pamela Becherini^{1,2}, Elisa Gelli¹, Samantha Ruberti¹, Katia Todoerti³, Luca Mastracci^{2,4}, Paola Contini⁵, Antonia Cagnetta², Antonella Laudisi^{1,2}, Fabio Guolo^{1,2}, Paola Minetto², Maurizio Miglino^{1,2}, Sara Aquino⁶, Riccardo Varaldo⁶, Daniele Reverberi⁷, Matteo Formica^{2,8}, Mario Passalacqua⁹, Alessio Nencioni^{2,5}, Antonino Neri^{3,10}, Mehmet K. Samur¹¹, Nikhil C. Munshi¹¹, Mariateresa Fulcinitti¹¹, Roberto M. Lemoli^{1,2†}, Michele Cea^{1,2*†}

¹ Clinic of Hematology, Department of Internal Medicine (DiMI), University of Genoa, Italy

² IRCCS Ospedale Policlinico San Martino, Clinic of Haematology, Genoa, Italy

³ Hematology, Fondazione Cà Granda IRCCS Policlinico, Milan, Italy

⁴ Department of Integrated Surgical and Diagnostic Sciences, University of Genoa, Italy

⁵ Department of Internal Medicine (DiMI), University of Genoa, Italy

⁶ Hematology and Hematopoietic Stem Cell Transplantation Unit, IRCCS Ospedale Policlinico San Martino, Genoa, Italy

⁷ U.O. Molecular Pathology, IRCCS Ospedale Policlinico San Martino, Genoa, Italy

⁸ Department of Surgical Sciences and Integrated Diagnostic (DISC), University of Genoa, Italy

⁹ Department of Experimental Medicine, University of Genoa, Italy

¹⁰ Department of Oncology and Haemato-oncology, University of Milan, Milan, Italy.

¹¹ Jerome Lipper Multiple Myeloma Center, Department of Medical Oncology, Dana Farber Cancer Institute, Harvard Medical School, Boston, Massachusetts.

† These are co-senior authors

***Corresponding Author:** Michele Cea, MD, Clinic of Haematology, Department of Internal Medicine and Specialities (DiMI), University of Genoa, Viale Benedetto XV n.6-16132 Genoa, Italy. Phone: 39-010-353-7970; fax: 39-010-353-38701; E-mail: michele.cea@unige.it

ACKNOWLEDGMENTS

The authors thank Dr. Jeremy Ryan and Prof. Anthony Letai for BH3 profiling experiments setup. They acknowledge also the MMRF for the access to CoMMpass study data.

FUNDING

This work was supported in part by the Associazione Italiana per la Ricerca sul Cancro (AIRC, MYFG #18491, IG #2328 to M.C. and MYFG # 21552 to A.C), Italian Ministry of Health (GR-2016-02361523 to A.C., and 5x1000 funds 2016 to M. C.) NIH grant P01-155258-07 (to M.F., M.K.S., and N.C.M.), Associazione Italiana Leucemie Linfomi e Mieloma (AIL sezione di Genova) and University of Genoa, Italy.

AUTHOR CONTRIBUTIONS

D.S. and M.C. designed the research, performed experiments, analyzed the data and wrote the manuscript; C.M., P.B, E.G., S.R., P.C. and D.R. performed experiments, and analyzed the data; P.B. performed mice experiments; L.M. performed IHC analyses; A.C., A.L., F.G., M.M., P.M., S.A., R.V., M.F. and Al.N. provided patient samples; M.P. performed immunofluorescence analysis; An.N., K.T., M. S., M.F. and N.M. performed genomic analyses; M.C and R.M.L. revised the final version of manuscript.

The authors have no competing financial interest to declare.

ABSTRACT

Identification of novel vulnerabilities in the context of therapeutic resistance is emerging as key challenge for cancer treatment. Recent studies have detected pervasive aberrant splicing in cancer cells, supporting its targeting for novel therapeutic strategies. Here, we evaluated the expression of several spliceosome machinery components in multiple myeloma (MM) cells and the impact of splicing modulation on tumor cell growth and viability. A comprehensive gene expression analysis confirmed the reported deregulation of spliceosome machinery components in MM cells, compared to normal plasma cells (PCs) from healthy donors, with its pharmacological and genetic modulation resulting in impaired growth and survival of MM cell lines and patient-derived malignant PCs. Consistent with this, transcriptomic analysis revealed deregulation of BCL2 family members, including decrease of anti-apoptotic long form of myeloid cell leukemia-1 (MCL1) expression, as crucial for “priming” MM cells for Venetoclax activity in vitro and in vivo, irrespective of t(11;14) status. Overall, our data provide a rationale for supporting the clinical use of splicing modulators as a strategy to reprogram apoptotic dependencies and make all MM patients more vulnerable to BCL2 inhibitors.

INTRODUCTION

Multiple Myeloma (MM) is a clonal B-cell malignancy characterized by excessive bone marrow plasma cells in association with monoclonal protein.^{1,2} MM is a heterogeneous disease driven by a large repertoire of molecular abnormalities, which contribute to its diverse clinical behavior. Currently available anti-MM therapies have remarkably improved patient outcome, but resistance is emerging as one of the foremost challenges in the clinical management of this tumor. Therefore, there is an unmet medical need to define biologic mechanisms of drug resistance, both to enhance efficacy of existing treatments and to facilitate the design of novel strategies.³ A fundamental feature of MM is its striking genomic instability leading to cancer development and clonal evolution.^{4,5} Consequently, the majority of studies have focused on changes in DNA: unfortunately, the greatest shortcoming of DNA-based approaches is their failure to capture the panoply of RNA editing events. Indeed, the genetic code is translated in the cell through the production of a messenger, mRNA, which usually has the same code of the DNA. A percentage of mRNAs are “edited”, so that although they are made as a faithful copy of the DNA, they are modified afterward to change the products of the genetic code. As a result, pre-mRNA processing by alternative splicing (AS) and/or RNA-specific deaminases, markedly increases the complexity of the human transcriptome.⁶ This process, which is executed in the nucleus by spliceosomes, occurs overwhelmingly in both normal and transformed cells, thus it is the rule rather than the exception. If this process is compromised, the resulting changes in splicing can lead to neoplastic transformation. Indeed, recent studies provide evidence that an abnormally expressed splicing factor machinery as well as its mutations can have oncogenic properties by impacting AS of genes associated with susceptibility and/or progression of cancer.⁷ Despite these intriguing findings, the global pattern of RNA processing in human cancer genomes has not been systematically characterized, and its functional importance and clinical relevance in cancer remains largely unknown. Thus, RNA

splicing deregulation represents an innovative and exciting area of research, in that it might be possible to modify or regulate RNAs as novel anti-cancer strategy.

AS is controlled by spliceosome, which is a dynamic molecular machine consisting of small nuclear RNAs (snRNA) and various protein complexes that cycle on and off from pre-mRNA during intronic splicing. This nuclear complex is composed of at least 170 proteins and five snRNAs associated with proteins forming the U1, U2, U4, U5, and U6 small nuclear ribonucleoproteins (snRNPs). It removes an intron from primary transcript and subsequently joins the exons by a trans-esterification reaction; the intron then undergoes debranching and is subsequently degraded.⁸ The accuracy of this process is essential for normal cellular function, whereas alternative splicing deregulation often occurs in tumors. As result, modulation of this tumor hallmark is now emerging as a promising strategy for anti-cancer therapies.^{9,10} Changes in alternative splicing are frequently caused by point mutations in the splicing factors such as SF3B1, which occurs in wide-range of tumors, including chronic lymphocytic leukemia (CLL), myelodysplastic syndromes (MDS), melanoma and breast cancers, resulting in aberrant splicing.¹¹⁻¹³ Also, MM cells harbor somatic alterations in this driver gene with missense mutations (K700 and K666) observed in about 1.7% of patients.¹⁴ Importantly, despite low mutational burden, recent studies suggest RNA splicing deregulation as driver mechanism for disease progression and drug-resistance occurrence as well.^{15,16} Here, we explored the impact of small molecule modulators of the spliceosome in perturbing tumor cells survival pathways and provide evidence for a novel combination strategy to treat MM.

METHODS

For a more detailed description of the methods used, see Supplementary Data.

Reagents

Meayamycin B and Sudemycin D6 (SD6) were kindly gifts from Prof. Kazunori Koide (University of Pittsburgh) and Prof. Thomas Webb (SRI Biosciences, Dept. of Chemistry and Biochemistry UCSC), respectively. E7107 was kindly provided by H3 Biomedicine, Inc.

Cell lines and primary tumor specimens

Cell lines were obtained from the ATCC or sources indicated in the Supplementary Materials.

Intracellular BH3 profiling

Intracellular BH3 (iBH3) profiling was performed as described in ¹⁷. Briefly, MM cells were pelleted and suspended in MEB buffer with addition of each BH3 peptide treatment with 0.002% w/v digitonin (MS1, mBAD and HRKy peptides were used). Mitochondria in the permeabilized cells were exposed to peptides for 45min at 26°C before fixation with 4 % formaldehyde at RT for 10 min. After addition of N2 neutralizing buffer for 15 minutes, cells were stained with Alexa Fluor® 488 Mouse anti-Cytochrome c (Clone 6H2.B4, BD Biosciences) 1:40 in 2% Tween20, 10% BSA PBS for 2 hours at RT and then ON at 4°C. The quantification of Cytochrome c loss induced by each peptide was evaluated by Flow cytometry (Navios 10/3, Beckman Coulter). Values indicate the percentage of Cytochrome c-negative cells calculated as in ¹⁷.

Transcriptome profiling, Alternative Splicing and Pathway analysis

RNA samples from H929 cells treated or not with Meayamycin B (3 nM, 8h) were obtained in duplicate for each condition, then extracted with the miRNeasy mini kit (Qiagen, #1038703) and processed using WT PLUS Reagent Kit, according to manufacturer's protocol (Thermo Fisher). Wide mRNA-transcriptome profiling was assessed using ClariomD Human array (Thermo Fisher). Robust

Multi Array (RMA) normalization on raw data, transcript annotation (Clariom_D_Human.r1.na36.hg38.a1.transcript) and Alternative Splicing Analysis were performed using Transcriptome Analysis Console (TAC 4.0) software (Thermo Fisher). Alternative Splicing events were identified in Meayamycin B-treated versus untreated H929 cells after filtering for transcripts expressed in both conditions, Exon expressed in at least one condition, Exon Splicing Index of at least 2 (<-2 or >2), Exon p-value <0.05 . Pathway enrichment analysis of significant alternative spliced genes was performed with the fgsea package in R together with BIOCARTA and REACTOME datasets. Significant pathways were selected based on FDR q-value $<25\%$. Global transcript expression levels were submitted on Gene Expression Omnibus (GEO) data repository, under GEO accession number GSE167042.

In vivo mouse models

All in vivo experiments were performed in accordance with the laws and institutional guidelines for animal care, approved by the Institutional Animal Care and Use Committee of University Hospital San Martino (protocol #473). Five weeks old female NOD/SCID J mice were acquired from Charles Rivers Laboratories (France) and were acclimatized for 3 weeks. $4,5 \times 10^6$ MM1S cells were injected subcutaneously in both flanks of the mouse. Treatment was initiated when the tumors reached a volume of about 50 mm^3 . In each experiment, mice were randomly divided to one of the following groups: control (vehicle); Venetoclax 100 mg/kg/day, dissolved in vehicle (60% phosal 50PG, 30% PEG 400, 10% ethanol) and administered by oral gavage; SD6 12 mg/kg/day, formulated in vehicle (10% hydroxypropyl-beta-cyclodextrin, HPCD, in phosphate buffer pH 7.4) and intra-tumorally injected; E7107 2,5 mg/kg/day prepared in vehicle (10% ethanol, 5% Tween-80, QS with saline) and intravenously injected (i.v.). Schedules are described in the individual figure legends. Tumor volume was calculated using the formula: tumor volume = $(w^2 \times W) \times \pi/6$, where “w” and “W” are “minor

side” and “major side” (in mm), respectively. Mice were sacrificed when the tumor reached a volume of about 1,5 cm³. Tumor masses were always isolated at the end of the experiment, weighted and fixed in 10% neutral buffered formalin (v/v) for histology.

RESULTS

Splicing machinery is markedly deregulated in MM and represents a disease aggressiveness biomarker. Genome-wide studies have recently demonstrated that deregulated expression of genes involved in splicing act as driver event for numerous tumors including MM.^{7,18} These data have prompted a growing interest for drugging the spliceosome machinery as novel strategy to improve anti-cancer therapies.¹⁴⁻¹⁶ We explored transcription levels of core small nuclear ribonucleoprotein (snRNP) assembly genes in primary MM cells from publicly-available collections of gene expression datasets by applying the KEGG spliceosome signature.^{14,19-21} A progressive transcriptional increase was observed in more advanced disease phases from monoclonal gammopathy of undetermined significance (MGUS) to plasma cell leukemia (PCL) and in HMCLs compared to normal plasma cells, indicating an association with tumor progression route (**Fig.S1, S2**). We confirmed higher expression in MM cells by gene expression analysis in primary cells from 7 additional MM patients and PBMCs from two healthy donors (**Fig.1A**). We next extended the analysis to the MMRF (MM Research Foundation) CoMMpass study that includes 774 MM patients^{5,22} profiled by RNA-sequencing by standardizing KEGG spliceosome signature with a z-score method,⁵ which stratified MM cases into three groups: low (n=303), intermediate (n=126) and high (n=345) (**Fig.1B**). Then we sought to explore any potential impact of aberrant spliceosome signature on clinical outcome and found that, in line with reported data¹⁶, patients in the high z-score group showed shorter progression free survival (PFS) and overall survival (OS) when compared with low-z score patients (median PFS 1300 versus 700 days, $P = 0.0017$; median survival not-reached versus 2000 days, $P=0.00027$) (**Fig.1C**). Importantly, a univariate Cox-model analysis confirmed spliceosome signature role in predicting OS ($p=0.0012$) and PFS ($p=0.0021$), similarly to ISS stage III ($p=0.0001$), 1q gain/amp ($p<0.0001$), del13q/RB1 ($p=0.0002$), and TP53 mutation occurrence ($p<0.0001$) (**Fig.1D** and **S3**). Overall, our transcriptome analyses

revealed a group of MM patients with higher upregulation in the RNA splicing machinery genes which correlated with poor prognosis. The spliceosome is a dynamic molecular machine consisting of several nuclear protein complexes, with the splicing factor SF3B1 responsible for on/off cycle of pre-mRNA during intronic splicing, essential for the correct functioning of this machinery. As result, western blot, immunohistochemistry and immunofluorescence analyses revealed high levels of SF3B1 on MM cell lines and CD138+ from patient-derived bone marrow biopsies (**Fig.1E, 1F, S4**) which was further increased upon interaction with bone marrow stromal cells (BMSCs) (**Fig.S5**) Notably, the greater SF3B1 protein level observed in tumor cells could be explained, at least in part, by the higher proliferation rate (in term of S and G2/M phases residing cells) of MM compared with healthy donor counterpart cells. (**Fig.S6**). Altogether these data suggest a role for spliceosome deregulation in MM growth.

Targeting the spliceosome core-element SF3B1 results in broad anti-MM activity.

Comprehensive RNA-seq based analyses have revealed profound and significant transcriptome changes, including alternative pre-mRNA splicing between MM and normal samples, with significant impact on overall clinical outcome.¹⁴ Despite that, SF3B1 somatic mutations, resulting in loss of function, occur in only 1.7% of MM patients, thus suggesting additional events accounting for the alterations observed in MM cells.¹⁵ Therefore, we evaluated the spectrum of alternatively spliced events (ASEs) in MMRF database, irrespective of SF3B1 mutation status. We classified the ASEs into five categories and analyzed the frequency of pattern changes according to SF3B1 expression level (top vs bottom quartile) (**Fig.2A**). Wide variability was observed, with alternative transcription start site (ATSS), intron retentions (IR) and alternative transcription termination site (ATTS) as the most abundant ASEs among the SF3B1 highly expressed group, indicating widespread spliceosome deregulation in MM, regardless of specific mutational profiling. Based on these data, we next

investigated SF3B1 role in these cells by genetic perturbation in a panel of MM cell lines. According to the reported activity of this factor in binding and splicing pre-mRNA,⁹ immunofluorescence analysis for the SR (serine/arginine-rich) protein SC-35 revealed a significant modulation of splicing machinery after SF3B1 knockdown (KD), with KD cells exhibiting reduced number of speckles which resulted larger and darker than control (**Fig.2B**). Importantly, SF3B1 KD not only affected splicing but also impaired MM cells viability by increasing apoptotic cell death in different MM cell lines and inducing caspase-3 and PARP1 cleavage as well (**Fig.2C** and **S7**). We subsequently tested the activity of the splicing modulator Meayamycin B in a panel of 14 MM cell lines, where we observed a significant decrease of cell viability with IC₅₀ values ranging from 0.49 to 3.5 nM (**Fig.2D, 2E**). Similar results were observed with additional splicing modulators such as Sudemycin D6 and E7107 (**Tab.S1**).^{23–25} The effect of Meayamycin B was next tested in primary MM cells, cultured in the absence or presence of bone marrow microenvironment. As seen in **Fig.2F, 2G** and **S8**, primary MM cells were significantly depleted after treatment with Meayamycin B, while a minimal toxicity was observed on normal components of the bone marrow milieu. These data support SF3B1 as a promising therapeutic target in MM.

Spliceosome deregulation affects genome stability of MM cells, irrespective of Myc status.

Genomic instability is a tumor hallmark resulting from deregulated DNA damage response, DNA repair defects, and failure of cell-cycle checkpoints. Recent studies have revealed that alternative splicing reprogramming after DNA damage responses relies on regulation of RNA-binding proteins (RBPs), which directly bind specific pre-mRNA and mRNA sequences and act as gatekeepers of genomic integrity. In this context, post-transcriptional RNA processing may add another layer of complexity to the maintenance of genomic stability in MM cells and targeting spliceosome during DNA damage response may represent an innovative approach to sensitize tumor cells to genotoxic

agents.²⁶ As shown in **Fig. 3A-3B**, we have observed that in SF3B1 KD MM cells increased DNA double-strand breaks and resulted in defective repair mechanisms as shown by accumulation of γ H2AX and reduced RAD51 levels, respectively. These changes were similarly observed after drug-treatment with Meayamycin B in a dose and time-dependent manner (**Fig. 3C-D**) and persist also after pre-incubation with pan-caspase inhibitor zVAD-fmk, thus suggesting a negligible role of apoptosis activation in the genomic instability triggered by spliceosome modulators (data not shown). Based on these data, we tested sensitivity of KD-SF3B1 MM cells to melphalan-induced DNA damage and, in line with previous studies,²⁶ we found that drug exposure led to increased γ H2AX induction, also in SF3B1-depleted cells, (data not shown) suggesting that huge spliceosome deregulation, triggered by SF3B1 targeting, accounts for the enhanced anti-MM activity of genotoxic stress. Recent genome-wide MYC-synthetic lethal screens have identified spliceosome components as candidate genes for synthetic lethality strategies, suggesting these as exploitable vulnerabilities for MYC-driven cancers.²⁷ To determine whether MYC presence correlates with Meayamycin B efficacy, we compared its protein level with the specific IC50 value measured for each tested cell line. As shown in **Figure 3E** no significant correlation ($R^2=0.1261$, $p=0.348$) was observed thus suggesting that Meayamycin B acts regardless of MYC protein level. Similarly, the ectopic expression of MYC in U266 MM cell lines increased γ -H2AX levels (**Fig. 3F**) but slightly enhanced the anti-MM activity of chemical or genetic SF3B1 targeting (**Fig. 3G, H**), thus confirming the marginal role played by this oncogenic program on anti-MM activity of splicing modulators.

Splicing inhibition remodels mitochondrial apoptotic dependencies in MM cells.

To shed light on the molecular mechanisms mediating the effects of splicing modulators on MM cell growth, we evaluated the transcriptomic profiles in MM cells treated with Meayamycin B. As shown in **Fig. 4A**, we observed increased AS events compared to untreated cells, with intron retention (IR) and

cassette exon (CE) as primary events across multiple targets (41.97 and 28.26%, respectively). Splicing outliers including alternative 5' and 3' donor site as well as complex events were observed less frequently. A comprehensive enrichment analysis of BioCarta annotated pathways was employed to identify cellular pathways affected by this treatment. Significant enrichment was observed among biological processes involved in regulation of cell-cycle, disease-progression, cell division and DNA replication, with apoptosis-related pathways identified as top-ranked events (**Fig. 4B**). A gene-level investigation, based on exon splicing index, revealed eleven genes of apoptosis pathway significantly mis-spliced: CHK1, BAX and BIRC3 were found to be interested by intron retention events, CASP10, CASP8 and CASP3 as affected by alternative cassette exons inclusion, PARP1 and MCL1 among targets with complex events and alternative 5'donor site, respectively (**Fig. 4C**). Moreover, we confirmed a significant change in MCL1 transcripts with depletion of the anti-apoptotic long isoform (MCL-1L), and accumulation of pro-apoptotic short isoform (MCL-1s) following exposure to both Meayamycin B and Sudemycin D6 (**Fig. S9**). Other BCL2 family genes, including BCL2 and BCLxL, were not affected (**Fig.4D**). A similar MCL-1 exon 2-skipped transcript occurred in SF3B1 silenced cells, with no modifications on BCL2 and BCLxL as well (**Fig. 4E**); these changes were also confirmed at protein level (**Fig. 4F**). Based on these data, we performed the intracellular BH3 (iBH3) profiling to investigate the mitochondrial apoptotic dependencies triggered by Meayamycin B or Sudemycin D6.²⁸ As shown in **Figure 4G** both inhibitors resulted in significant increase of cytochrome c release following exposure to mBAD and HRK-y BH3 peptides, indicating a functional shift in mitochondrial dependencies from MCL1 towards BCL2/BCLxL anti apoptotic members.

Splicing modulations increases sensitivity of MM cells to the BCL2 inhibitor Venetoclax.

Cancer cells are dependent on multiple anti-apoptotic proteins to promote their survival, therefore targeting more than one protein results in synergistic effects in several preclinical models of solid and

hematological tumors.^{29–32} In such a scenario, the dysregulated expression of BCL2 family members observed after splicing modulators treatment, prompted us to harness apoptosis as strategy for enhancing anti-MM activity of these agents. We therefore evaluated the ability of splicing modulators to enhance effects of the BCL2 specific inhibitor Venetoclax against MM cell growth and survival. Low dose of this BH3-mimetic and Meayamycin B or Sudemycin D6 combo was synergistic in several MM cells, including those carrying t(11;14), which has been reported to affect anti-MM activity of Venetoclax. (**Fig. 5A-B** and **S10-11**).³³ As result, PARP1 and caspase 3 cleavage occurred after these stimuli at much extent compared with single agent exposure (**Fig. 5C**). These results were also confirmed in SF3B1 KD MM cells (**Fig. 5D**). We next examined the effects of the combination therapy on primary plasma cells (PCs) collected from MM patients: as shown in **Fig. 5E** we confirmed the increased sensitivity to Venetoclax of MM PCs exposed to SD6 compared with single agent treatment, regardless of specific stage-disease, cytogenetic abnormalities, or previous drug-exposure. Importantly, no significant effects were observed on PBMCs derived from the same MM patients, suggesting tumor specificity of drugs combination. The impact of this strategy was finally tested on primary MM cells in the presence of their bone-marrow microenvironment with slight toxicity observed on normal bone marrow components (**Fig. 5F** and **S12**). To strengthen clinical relevance of our findings, we next screened different agents currently used for MM treatment in combination with splicing modulators, by performing head-to-head comparison analysis. As shown in Fig. **S13**, Venetoclax was readily identified as the best sensitizer of MM cells to Meaymicin B activity with a Combination Index resulting to be lowest among tested drugs. Collectively, these data support splicing modulation as a strategy to increase Venetoclax sensitivity of MM cells. Based on these results, we next moved on drug resistance mechanisms by investigating whether splicing pathways affect Venetoclax resistance of MM cells. To this aim, we assessed a panel of 10 MM cell lines and measured absolute half-maximal inhibitory

concentrations (IC₅₀) to capture the efficacy and potency of the drug (**Fig. 5G**). We then listed all cell lines according to Venetoclax sensitivity and used CCLE RNA-seq data to compare gene expression profiling of resistant versus sensitive cell lines; significant de-regulated genes were submitted to the GSEA software to find most affected pathways. Importantly, this analysis revealed that gene sets associated with RNA biology, RNA processing, and splicing pathways, were strongly enriched in sensitive cell lines, based on negative normalized enriched score (NES) and low q-value, thus supporting their link with venetoclax-sensitivity (**Fig. 5H**).

Splicing inhibitors synergize with Venetoclax in vivo in humanized MM murine models.

We finally evaluated the efficacy of the combination regimen in vivo in MM xenograft murine models. In the first model, mice were treated with Venetoclax (100 mg/kg, oral administration, once a day for 15 days) and SD6 (12 mg/kg, intratumorally, once a day for 10 days) alone or in combination. SD6 dosing was chosen based on previously reported efficacy and safety profiles in xenograft lymphoma models, while Venetoclax was used at 100 mg/kg to reduce its potency as single agent. Treatment was well tolerated during the 2-weeks treatment (**Fig. S14**). The superior effect of the combination over single agents in reducing tumor volume and weight, (**Fig. 6A-B**) was observed starting after 1 week of therapy. The decrease in tumor growth was associated with improved overall survival of animals treated with the combination therapy, as compared with vehicle and single agents (**Fig. 6C**, $p < 0.05$). Remarkably, animals treated with Venetoclax monotherapy had a similar survival to that of vehicle-treated animals ($p = 0.15$), confirming the lack of sensitivity of this model to Venetoclax treatment alone. In line with this data, immunohistochemical analyses revealed a dramatic increase of cleaved caspase-3 positive MM cells, with marked reduction of mitotic percentage (**Fig. 6D, E**). Additionally, increased apoptotic bodies were observed in tumors derived from mice treated with combination (**Fig. 6E**). We also evaluated *in-vivo* efficacy of Venetoclax combination with the clinical grade SF3b-

targeting splicing modulator E7107.³⁴ Mice injected with human MM1S cells were treated with vehicle, E7107 (2.5 mg/kg intravenous, once a day for 5 days), Venetoclax (100 mg/kg oral administration, once a day for 5 days) and their combination. As observed in our previous model, E7107-treated tumors resulted in significant tumor regression compared to control mice and mice treated with Venetoclax alone and, the effect of E7107 was further enhanced by the combination with Venetoclax, as shown in **Fig.6F** ($P<0.05$). The mean tumor volume of mice treated with combination was lower than single agent treated mice bearing tumors with higher activity at day 54. Improved outcome was also observed for the combination group of mice, with a median survival significantly longer compared to those treated with vehicle or monotherapies (combo vs vehicle $P<0.05$; combo vs Venetoclax $P<0.001$; combo vs E7107 $P<0.05$) (**Fig. 6G**). Overall, these data support the potential benefits of splicing inhibition to enhance anti-MM effects of Venetoclax.

DISCUSSION

The process of RNA splicing regulates gene function in normal cells, but only recently its deregulation has been implicated in driving the development and/or maintenance of cancer.^{9,35} Indeed, comprehensive genomic analyses have revealed accumulation of transcriptome changes, including aberrantly spliced products during tumor progression and drug-resistance occurrence, thus identifying spliceosome machinery deregulation as crucial for tumor cells growth and making its targeting an innovative strategy for successful anti-cancer approaches.⁹ In such a context, small molecules including spliceostatin, sudemycins, pladienolide and its derivatives are emerging as groundbreaking tools to fight cancers, especially those bearing splicing genes mutations. Since RNA splicing apparatus is frequently affected by wide range of driving events, including oncogenic MYC-activation and MCL1 addiction, a synthetic-lethal relationship between different tumor “Achille’s heel” and core-spliceosome inhibition has been proposed, resulting in increased use of splicing modulators for cancer treatment.^{9,19,27,36}

Here, we first confirmed the already reported upregulation of alternative splicing processes in MM cells by analyzing clinically annotated high throughput RNA-seq data from CoMMPass study. A pervasive splicing aberration was found in these cells to be associated with aberrant expression of RNA splicing machinery components and significantly impacts on overall clinical outcome. In line with these data, proliferating MM cells exhibited greater levels of spliceosome component SF3B1 than normal cells suggesting its role for tumor cell growth. Alternative splicing affects wide range of genes with prevalent impairment of various cellular processes, including cell cycle. Indeed, splicing isoforms have been reported for key cell-cycle factors including cell division cycle 25 (CDC25), aurora kinase B (AURKB), CDC-Like kinase 1 (CLK1) and CDK2.^{37,38} Thus, tumor cells proliferation rate might be responsible for high SF3B1 levels observed in these cells, but more investigations are need. Despite the

low mutational burden reported for splicing factors in MM, a striking anti-tumor effects of splicing modulators was observed associated with a significant change in MCL1 spliced isoforms in treated cells than specific control. These results are in accordance with other reports showing differential sensitivity to splicing modulation in BCL2 family genes, providing novel insights into mechanisms for spliceosome-targeted based approaches in tumors.²⁹ The effect on MCL1 caused by SF3B1 targeting resulted in a cellular addiction shifting from MCL1 to BCL2 thus providing a rationale for combination of splicing modulators with the BCL2 inhibitor Venetoclax to achieving a synergistic activity against MM cell growth and viability. Indeed, a significant impact of this combination was observed on MM cells both *in vitro* and *in vivo*, while sparing non-cancerous cells thus providing evidence for a favorable therapeutic index.

Apoptosis is a highly regulated intracellular process, essential for normal cells survival and development; defects in regulation of this process result in a number of abnormalities, including cancer.³⁹ Several B-cell malignancies such as chronic lymphocytic leukemia (CLL), lymphomas and plasma cell neoplasms, present different interaction between subgroups of the BCL2-family members including the pro-survival BCL2 (BCL2, MCL1, BCL2A1 and BCLxL) and the BH3-only proteins causing apoptosis. In these tumors, drug exposure results in perturbed intrinsic apoptotic pathway with mitochondrial apoptotic dependencies reprogramming and cell-death evasion. A proof-of-concept for this strategy is represented by the breakthrough small molecules mimicking BH3-only proteins, which have totally changed the treatment landscape of CLL and Acute Myeloid Leukemia.⁴⁰ Also MM exhibit high dependence on apoptosis as suggested by efficacy of phase I clinical trial with Venetoclax in monotherapy (NCT02755597) in RRMM patients, mainly in those harboring the t(11;14) translocation.³³ Unfortunately, changes in apoptosis regulators result in clinical resistance, thus supporting alternative strategies for these patients, including multiple apoptotic proteins inhibition.^{41,42}

40% of MM patients harbor gain or amplification status of 1q21 which makes these cells addicted to MCL1 and extremely vulnerable to its targeting, as suggested by preclinical studies.^{30,43} However, MCL1 has proven to be more challenging to target than BCL2, despite the long-standing interest in designing potent and selective MCL1 inhibitors for therapeutic use that have resulted in poor clinical benefits with few trials still ongoing (NCT02992483, NCT02675452 and NCT03465540). We demonstrate here that modulation of splicing by selectively targeting MCL1, results in enhanced BCL2 activity on MM cells, and supports the synergistic activity observed in combination with Venetoclax. Remarkably, no significant effects were observed on non-tumor cells derived from the same MM patient and treatment was well tolerated in mice as well, suggesting safe therapeutic window of tested combinations. Emerging studies suggest that tumor cells, including MM, hijack spliceosome activity to evade anti-tumor therapies: mis-spliced forms of binding protein CRBN and broad-scale intron retention have been observed in MM patients with IMiDs or PIs resistance occurrence, respectively.^{16,44} Thus, splicing interference represents an exploitable vulnerability to overcome drug resistance but still deserves further investigations. Here, we confirm that alternative splicing is largely perturbed in MM cells and constitutes an attractive source for novel therapeutic strategies. Low dose of splicing modulators, by shifting apoptotic dependencies, results in enhanced BH3 mimetic Venetoclax susceptibility, irrespective of specific genomic landscapes including splicing factor-mutations, c-MYC-expression or t(11;14) status, providing rationale for the use of this combination for the treatment of all MM patients.

REFERENCES

1. Palumbo A, Anderson K. Multiple Myeloma. *N Engl J Med*. 2011;364(11):1046-1060.
2. Kumar SK, Rajkumar V, Kyle RA, et al. Multiple myeloma. *Nat Rev Dis Prim*. 2017;3(1):17046.
3. Leung-Hagesteijn C, Erdmann N, Cheung G, et al. Xbp1s-Negative Tumor B Cells and Pre-Plasmablasts Mediate Therapeutic Proteasome Inhibitor Resistance in Multiple Myeloma. *Cancer Cell*. 2013;24(3):289-304.
4. Cea M, Cagnetta A, Adamia S, et al. Evidence for a role of the histone deacetylase SIRT6 in DNA damage response of multiple myeloma cells. *Blood*. 2016;127(9):1138-1150.
5. Soncini D, Minetto P, Martinuzzi C, et al. Amino acid depletion triggered by α -asparaginase sensitizes MM cells to carfilzomib by inducing mitochondria ROS-mediated cell death. *Blood Adv*. 2020;4(18):4312-4326.
6. Ast G. How did alternative splicing evolve? *Nat Rev Genet*. 2004;5(10):773-782.
7. Graubert TA, Shen D, Ding L, et al. Recurrent mutations in the U2AF1 splicing factor in myelodysplastic syndromes. *Nat Genet*. 2012;44(1):53-57.
8. Krämer A. The structure and function of proteins involved in mammalian pre-mRNA splicing. *Annu Rev Biochem*. 1996;65:367-409.
9. Lee SCW, Abdel-Wahab O. Therapeutic targeting of splicing in cancer. *Nat Med*. 2016;22(9):976-986.
10. Webb TR, Joyner AS, Potter PM. The development and application of small molecule modulators of SF3b as therapeutic agents for cancer. *Drug Discov Today*. 2013;18(1-2):43-49.
11. Yoshida K, Sanada M, Shiraishi Y, et al. Frequent pathway mutations of splicing machinery in myelodysplasia. *Nature*. 2011;478(7367):64-69.

12. Quesada V, Conde L, Villamor N, et al. Exome sequencing identifies recurrent mutations of the splicing factor SF3B1 gene in chronic lymphocytic leukemia. *Nat Genet.* 2012;44(1):47-52.
13. Maguire SL, Leonidou A, Wai P, et al. SF3B1 mutations constitute a novel therapeutic target in breast cancer. *J Pathol.* 2015;235(4):571-580.
14. Bauer MA, Ashby C, Wardell C, et al. Differential RNA splicing as a potentially important driver mechanism in multiple myeloma. *Haematologica.* 2021;106(3):736-745.
15. Walker BA, Mavrommatis K, Wardell CP, et al. Identification of novel mutational drivers reveals oncogene dependencies in multiple myeloma. *Blood.* 2018;132(6):587-597.
16. Huang HH, Ferguson ID, Thornton AM, et al. Proteasome inhibitor-induced modulation reveals the spliceosome as a specific therapeutic vulnerability in multiple myeloma. *Nat Commun.* 2020;11(1):1931.
17. Ryan J. A Guide to BH3 Profiling METHOD 2: iBH3 PROFILING. 2017.
18. Adamia S, Bar-Natan M, Haibe-Kains B, et al. NOTCH2 and FLT3 gene mis-splicings are common events in patients with acute myeloid leukemia (AML): New potential targets in AML. *Blood.* 2014;123(18):2816-2825.
19. Koh CM, Bezzi M, Low DHPP, et al. MYC regulates the core pre-mRNA splicing machinery as an essential step in lymphomagenesis. *Nature.* 2015;523(7558):96-100.
20. Adamia S, Abiatari I, Amin SB, et al. The effects of MicroRNA deregulation on pre-RNA processing network in multiple myeloma. *Leukemia.* 2020;34(1):167-179.
21. Zamani-Ahmadm Mahmudi M, Dabiri S, Nadimi N. Identification of pathway-based prognostic gene signatures in patients with multiple myeloma. *Transl Res.* 2017;185:47-57.
22. Laganà A, Perumal D, Melnekoff D, et al. Integrative network analysis identifies novel drivers of pathogenesis and progression in newly diagnosed multiple myeloma. *Leukemia.*

2018;32(1):120-130.

23. Kotake Y, Sagane K, Owa T, et al. Splicing factor SF3b as a target of the antitumor natural product pladienolide. *Nat Chem Biol.* 2007;3(9):570-575.
24. Kaida D, Motoyoshi H, Tashiro E, et al. Spliceostatin A targets SF3b and inhibits both splicing and nuclear retention of pre-mRNA. *Nat Chem Biol.* 2007;3(9):576-583.
25. Folco EG, Coil KE, Reed R. The anti-tumor drug E7107 reveals an essential role for SF3b in remodeling U2 snRNP to expose the branch point-binding region. *Genes Dev.* 2011;25(5):440-444.
26. Marchesini M, Ogoti Y, Fiorini E, et al. ILF2 Is a Regulator of RNA Splicing and DNA Damage Response in 1q21-Amplified Multiple Myeloma. *Cancer Cell.* 2017;32(1):88-100.
27. Hsu TYT, Simon LM, Neill NJ, et al. The spliceosome is a therapeutic vulnerability in MYC-driven cancer. *Nature.* 2015;525(7569):384-388.
28. Certo M, Moore VDG, Nishino M, et al. Mitochondria primed by death signals determine cellular addiction to antiapoptotic BCL-2 family members. *Cancer Cell.* 2006;9(5):351-365.
29. Ruefli-Brasse A, Reed JC. Therapeutics targeting Bcl-2 in hematological malignancies. *Biochem J.* 2017;474(21):3643-3657.
30. Kotschy A, Szlavik Z, Murray J, et al. The MCL1 inhibitor S63845 is tolerable and effective in diverse cancer models. *Nature.* 2016;538(7626):477-482.
31. Moujalled DM, Pomilio G, Ghiurau C, et al. Combining BH3-mimetics to target both BCL-2 and MCL1 has potent activity in pre-clinical models of acute myeloid leukemia. *Leukemia.* 2019;33(4):905-917.
32. Prukova D, Andera L, Nahacka Z, et al. Cotargeting of BCL2 with venetoclax and MCL1 with S63845 is synthetically lethal in vivo in relapsed mantle cell lymphoma. *Clin Cancer Res.*

2019;25(14):4455-4465.

33. Kumar S, Kaufman JL, Gasparetto C, et al. Efficacy of venetoclax as targeted therapy for relapsed/refractory t(11;14) multiple myeloma. *Blood*. 2017;130(22):2401-2409.
34. Hong DS, Kurzrock R, Naing A, et al. A phase I, open-label, single-arm, dose-escalation study of E7107, a precursor messenger ribonucleic acid (pre-mRNA) splicesome inhibitor administered intravenously on days 1 and 8 every 21 days to patients with solid tumors. *Invest New Drugs*. 2014;32(3):436-444.
35. Chen S, Benbarche S, Abdel-Wahab O. Splicing factor mutations in hematologic malignancies. *Blood*. 2021;138(8):599-612.
36. Aird D, Teng T, Huang C-L, et al. Sensitivity to splicing modulation of BCL2 family genes defines cancer therapeutic strategies for splicing modulators. *Nat Commun*. 2019;10(1):137.
37. Petasny M, Bentata M, Pawellek A, et al. Splicing to Keep Cycling: The Importance of Pre-mRNA Splicing during the Cell Cycle. *Trends Genet*. 2021;37(3):266-278.
38. Jorge J, Petronilho S, Alves R, et al. Apoptosis induction and cell cycle arrest of pladienolide B in erythroleukemia cell lines. *Invest New Drugs*. 2020;38(2):369-377.
39. Hanahan D, Weinberg RA. The hallmarks of cancer. *Cell*. 2000;100(1):57-70.
40. DiNardo CD, Jonas BA, Pullarkat V, et al. Azacitidine and Venetoclax in Previously Untreated Acute Myeloid Leukemia. *N Engl J Med*. 2020;383(7):617-629.
41. van Delft MF, Wei AH, Mason KD, et al. The BH3 mimetic ABT-737 targets selective Bcl-2 proteins and efficiently induces apoptosis via Bak/Bax if Mcl-1 is neutralized. *Cancer Cell*. 2006;10(5):389-399.
42. Gupta VA, Barwick BG, Matulis SM, et al. Venetoclax sensitivity in multiple myeloma is associated with B cell gene expression. *Blood*. 2021;137(26):3604-3615.

43. Slomp A, Moesbergen LM, Gong JN, et al. Multiple myeloma with 1q21 amplification is highly sensitive to MCL-1 targeting. *Blood Adv.* 2019;3(24):4202-4214.
44. Gooding S, Ansari-Pour N, Towfic F, et al. Multiple cereblon genetic changes are associated with acquired resistance to lenalidomide or pomalidomide in multiple myeloma. *Blood.* 2021;137(2):232-237.

FIGURE LEGENDS

Figure 1. Splicing machinery is markedly deregulated in MM. **A)** Heat map showing expression levels (row z-score) of indicated genes among plasma cells derived from patients with multiple myeloma (n=7) and healthy individuals (n=2). The color scale spans the relative gene expression changes standardized on the variance. **B)** Heatmap of 774 multiple myeloma patients included in CoMMpass study ordered in three groups according to z-score calculated on 124 genes of KEGG spliceosome gene set, as annotated in MSigDB. **C)** Kaplan–Meier survival curves of high z-score (red) and low z-score (blue) MM patients of CoMMpass cohort (642 patients analyzed) on PFS and OS data. Log-rank test p-value and number of samples at risk in each group across time are reported. **D)** Forest plot based on Cox univariate analysis for overall survival. Squares represent hazard ratios; bars represent 95% confidence intervals. **E)** Protein lysates from a panel of MM cell lines (HMCLs) and primary MM patients or healthy donors were analyzed for SF3B1 expression by WB. GAPDH was used as loading control. One representative experiment is shown. **F)** Representative images of SF3B1 and CD138 immunocytochemistry stain in BM from MM patients (n=5). Conventional Giemsa staining is also shown. Original magnification $\times 200$, scale bar, 100 μm

Figure 2. Spliceosome core-element SF3B1 targeting results in anti-MM activity. **A)** Percentage of indicated splicing categories across RNA-seq data derived from CoMMpass study according to SF3B1 expression levels (top vs bottom quartile). **B)** Immunofluorescence staining for SC-35 in scramble and SF3B1-sh RNA H929 MM cells. SF3B1 silencing was validated by Western Blot as shown in the panel below. SC-35 staining of nuclear speckles is shown: Fluorescence Intensity (MFI) per cell/nucleus of the specific signal was quantified by counting at least 50 nuclei per condition as reported in the histogram below (**p= 0.0042, two-sided Student t-test). Scale bar, 10 μm **C)** MTS assay of MM1S (top) and H929 (bottom) lentivirally transduced with shSF3B1 (#1, #2 and #3) or sh scramble. Cell

viability was measured at indicated time point after transduction. Western blot analyses were performed at day 3, confirming decreased SF3B1 protein levels and apoptotic cell death features (PARP1 and Caspase 3 cleavage). Data are representative of at least three independent experiments. **D)** Cell viability curves compare a panel of 14 MM cell lines' sensitivity to Meaymicin B (nM) for 48 h (n = 3 technical replicates; mean \pm S.D.) **E)** Evaluation of PARP, caspase 3, MCL1 and GAPDH by western blot on indicated MM cell lines treated with increasing doses of MeaymicinB for 24hours. **F)** Treatment of primary bone marrow aspirate samples from MM patients (n=5) at various doses of MeaymicinB (0.1-30 nM) for 48 hours shows significant cytotoxicity of CD138+ tumor cells (n = 3 technical replicates; mean \pm S.D.). **G)** ex vivo evaluation of Meaymicin B in total bone marrow cells from one representative MM patient. After red cell lysis, cells were stained with Annexin V, DAPI and CD38 mAb to identify viable as well as apoptotic myeloma (CD38 positive/CD45 negative) and normal (CD38 negative/CD45 negative) cells.

Figure 3. Spliceosome deregulation affects genome stability of MM cells irrespective of Myc status **A)** Detection of γ H2AX and Q-nuclear was measured by confocal microscopy in H929 cells expressing shRNA (clone #3 and #4) targeting SF3B1 or control. Each panel includes representative foci-containing cells graph, over three experiments. (** p= 0.004, *** p<0.001; two-sided Student t-test). **B)** H929 cells were engineered to express an anti-SF3B1 shRNA (3 clones). Next, SF3B1, RAD51 and γ H2AX protein levels were detected by immunoblotting. **C)** Detection of γ H2AX and Q-nuclear by confocal microscopy of H929 cells ex cultured with or without increased dosed of Meayamycin B (1-3 μ M) for 24 h. Each panel includes representative foci-containing cells graph, over three experiments (* p= 0.01, **** p<0.0001; two-sided Student t-test). (**A, C**) scale bar, 50 μ m **D)** Western blot analysis of DNA damage response markers (RAD51 and γ H2AX) after Meaymicin B treatment over a range of doses (*upper panel*) and timing (*lower panel*) in H929 cells. **E)** Relative

expression of Myc protein plotted versus Meaymicin B cytotoxicity IC50 values. The Pearson correlation coefficient (r) and the P value, calculated using GraphPad Prism Version 5 analysis software, are indicated; **F**) immunoblot for cMyc, SF3B1 and γ H2AX protein levels in isogenic U266 cells (pLV empty) or cMyc overexpressing (pLV cMyc) cells; **G**) these cells were treated with growing doses of Meayamycin B for 48h. Cell viability was measured with MTS assay and presented as a percentage of control. **H**) Cell viability analysis of pLV empty pLV cMyc) U266 cells transduced with shRNAs clones containing the target sequence of SF3B1 (clone#1) or scrambled control. (** p= 0.004; two-sided Student t-test).

Figure 4. BCL2 family member deregulation outlines splicing modulators activity on MM cells.

A) Pie chart showing the proportion of significant splice changes derived from ClariomD data of MM cell lines treated with Meayamycin B compared with DMSO-treated controls. Yellow slice indicates significant intron cassette exon events; purple slice indicates significant intron retention events; gray indicate all other complex categories of splice events. **B)** The top ten pathways included in BioCarta gene sets enriched by fgsea R package among the 1,000 most significant mis-spliced genes in Meayamycin B treated cells. **C)** Bubble plot shows the enrichment scores, p-values and the types of aberrant splicing event in the top mis-spliced genes of apoptosis pathway after Meayamycin B treatment compared with control cells. **D-E)** RT-PCR analyses of H929 cells after 6-hour treatment with growing doses of Meayamycin B (3-6 nM) and Sudemycin D6 (1-3 μ M) (**D**) or different time points after lentiviral transduction with scramble control or SF3B1 specific shRNAs clone#1 (**E**), to assess levels of MCL1 (L, long and S, short isoforms), BCLxL and BCL2. GAPDH is used as internal control. The length of the main amplified isoforms is indicated as base pairs (bp). **F)** Western blot analysis of MCL1, BCL2, BCLxL, PARP and cleaved caspase3 protein expression upon treatment with Meayamycin B and SD6 in H929 cells. GAPDH was used as loading control. **G)** Heatmap of

percentage cytochrome c loss, as quantified by flow cytometry on indicated MM cell lines after 6 hours of treatment with different chemicals as compared with DMSO-treated controls (purple, lowest value; yellow, highest value). After each treatment, MM cells were exposed to BH3 mimetic peptides (MS1 10uM, mBAD and HRKy 100uM for all cell lines except for MM1S where 50 μ M mBAD and HRKy were used) for 45 minutes at room temperature and subsequently stained for FACS analysis.

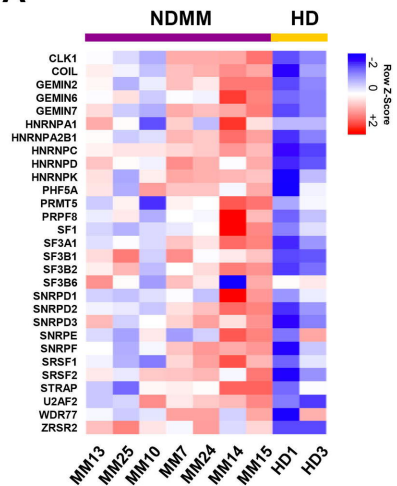
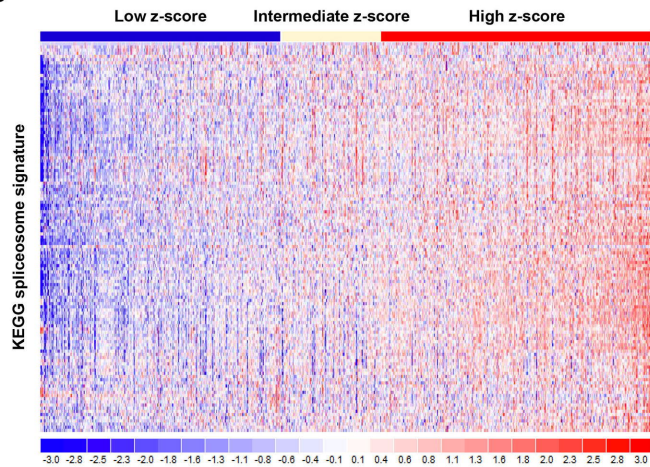
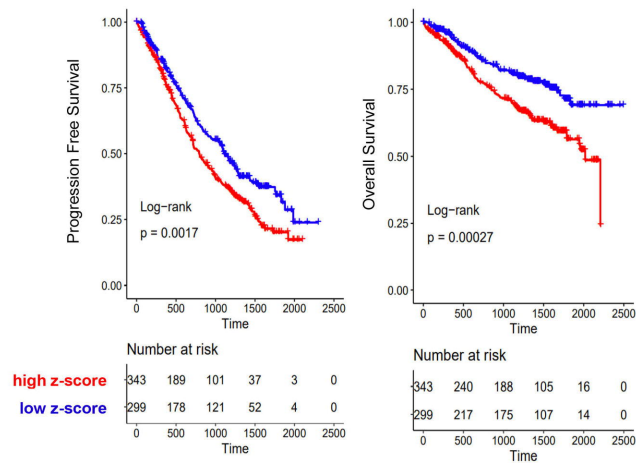
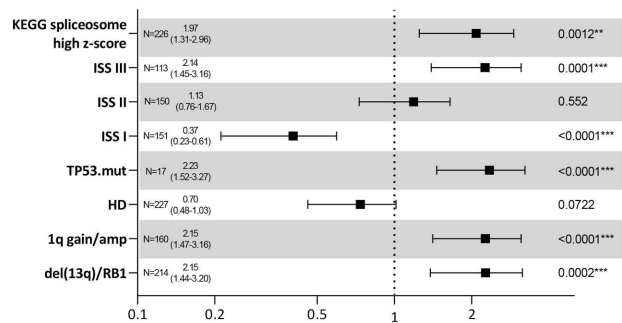
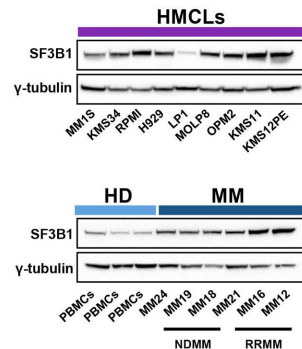
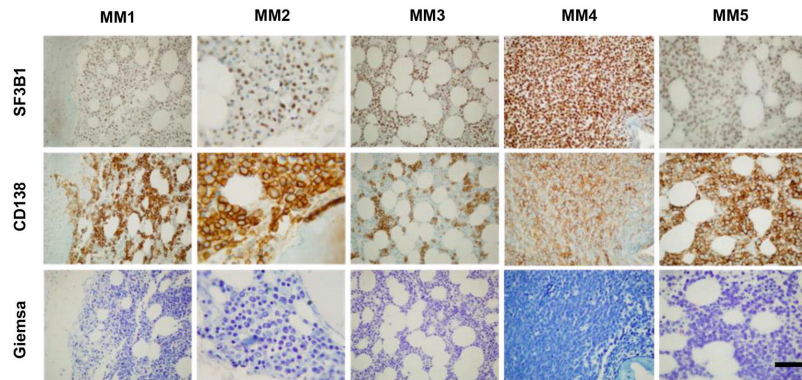
Figure 5. Splicing modulators sensitizes MM cells to Venetoclax by deregulating BCL2 family-members. Cell viability curves of MM cells treated with combination therapies using Meayamycin B (A) or Sudemycin D6 (B) and Venetoclax. CI synergy score (calculated with CalcuSyn software) for each set of drugs combination is indicated. Data are presented as mean \pm S.D (n=3). (*** $p \leq 0.01$, **** $p \leq 0.001$; unpaired t test). C) Immunoblots for phospho-SF3B1, SF3B1, PARP, caspase 3, and GAPDH on MM cell lines following each stimulus (indicated in figure) at 24 hours. D) Apoptotic cell death assessed with flow cytometry analysis after Annexin V/PI staining of AMO-1 cells SF3B1-silenced (nucleofected with specific siRNAs) or control cells (siRNA scramble) treated with Venetoclax (7.5 μ M) for 48 hours. Displayed are data represented as mean \pm SD in all (n = 3). E) CD138+ cells (*left*) and PBMCs (*right*) collected from MM patients were treated with indicated doses of SD6, Venetoclax (0.5 μ M) and their combination for 48 hours. Cell viability was measured by CTG assay. Cells deriving from the same patient are represented with same color in each graph. F) Flow plots of one representative MM patient sample. Corresponding sensitivity of MM-gated cells (CD38+/CD45-) and BMSCs (CD38-/CD45-) to Venetoclax, SD6 and cotreatment are shown. G) Indicated HMCLs (n=10) were treated with different doses of Venetoclax (Ven) for 24 h and cell survival was assessed by CTG. IC₅₀ analysis was performed with GraphPad software. n=3 independent experiments. H) GSEA Normalized enriched scores (NES) and FDR q-values for top enriched pathways, according to Reactome gene set, among de-regulated genes of Venetoclax resistant

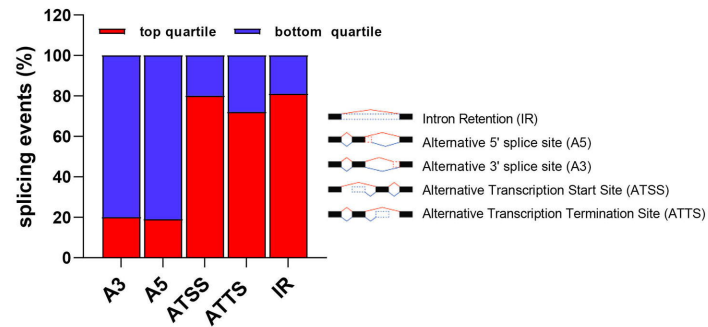
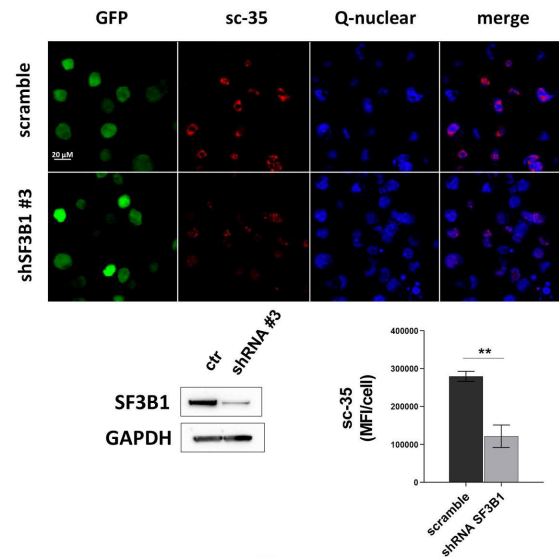
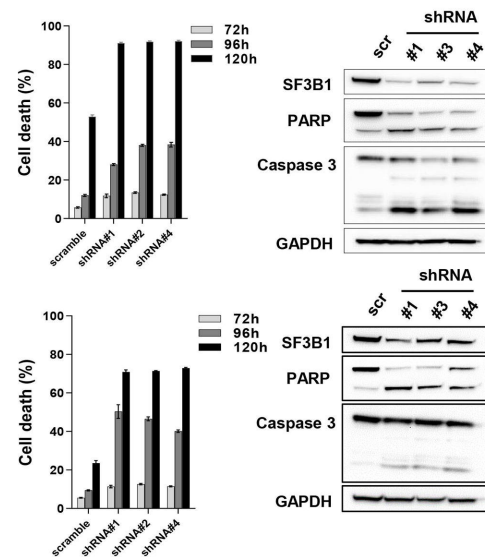
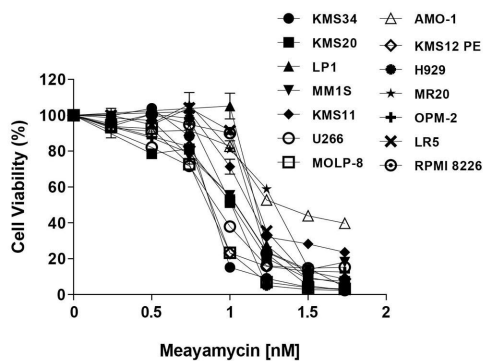
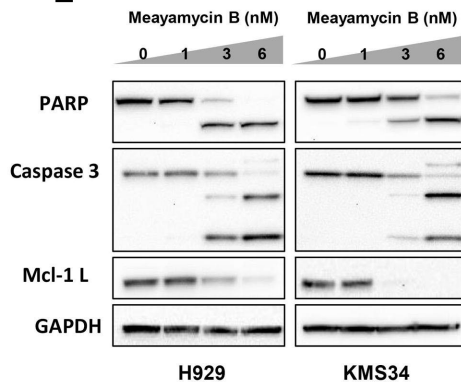
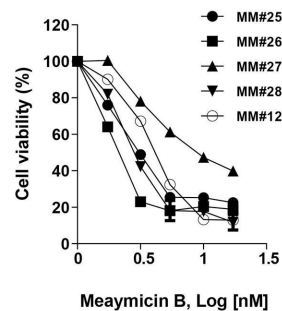
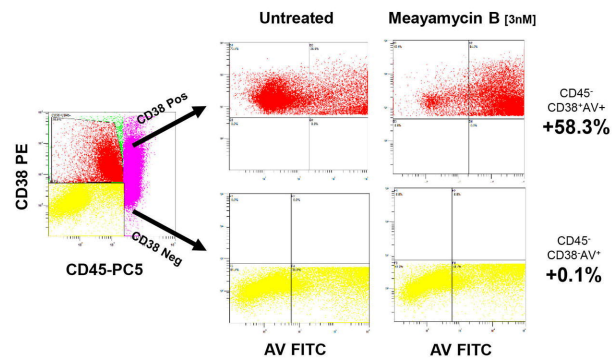
vs sensitive cell lines; red square indicates the most significant region with splicing-related pathways accumulation (*left*); examples of GSEA-derived enrichment plots for genes involved in the splicing machinery (*right*).

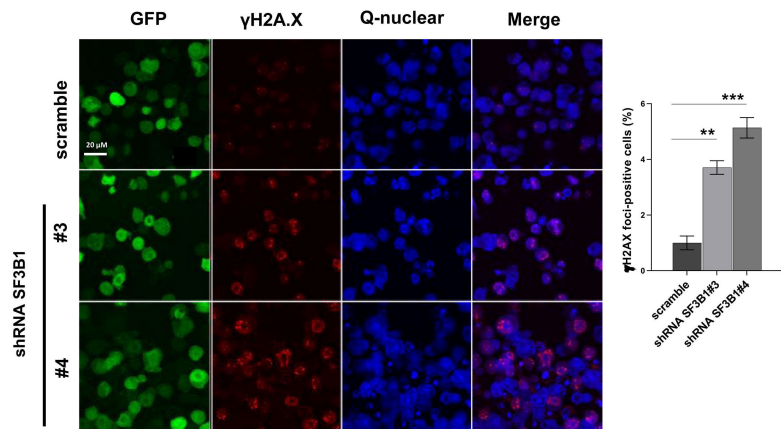
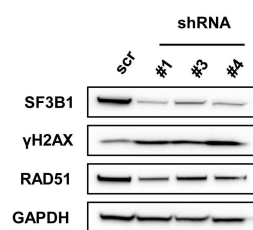
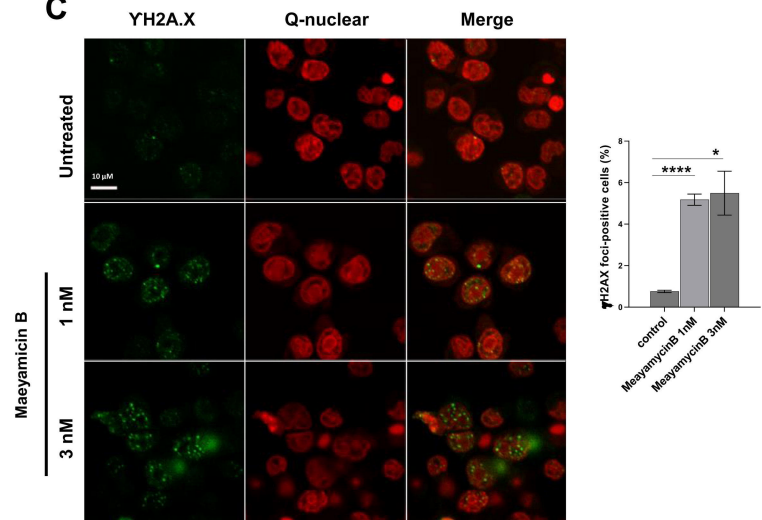
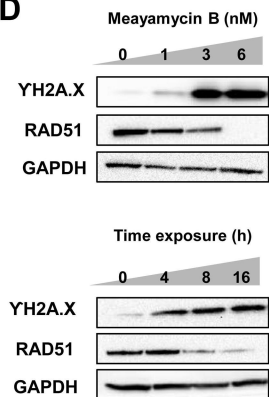
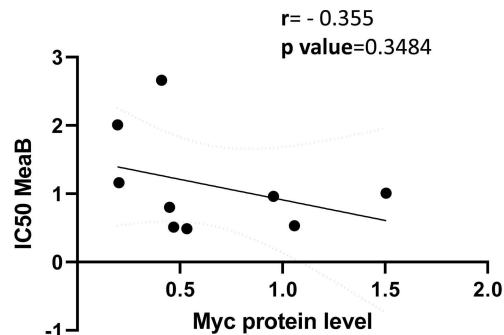
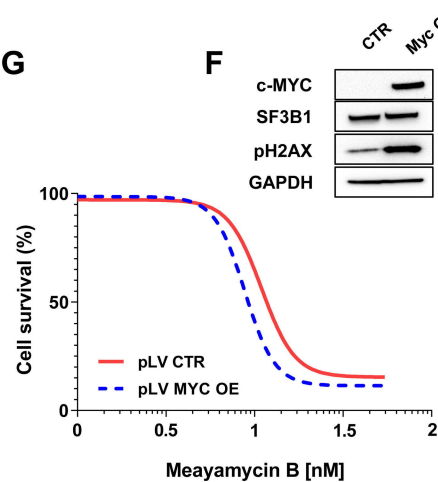
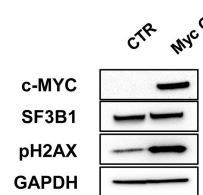
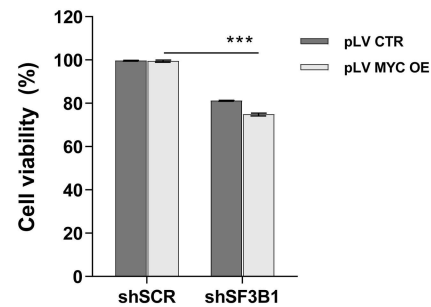
Figure 6. Splicing inhibitors synergize with Venetoclax in vivo in humanized MM murine models

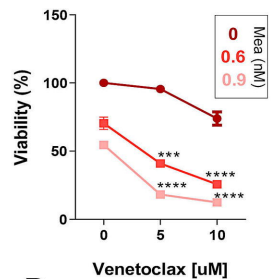
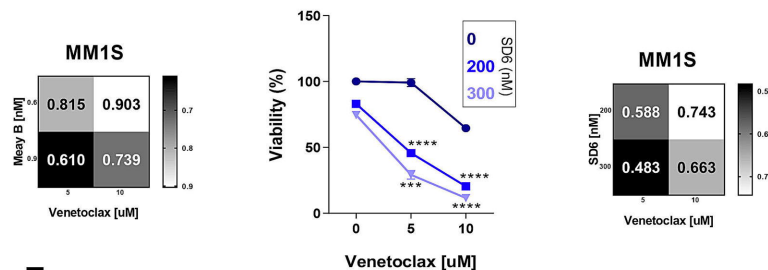
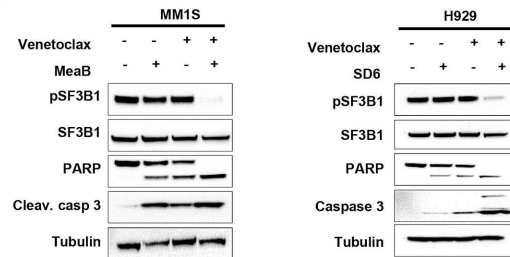
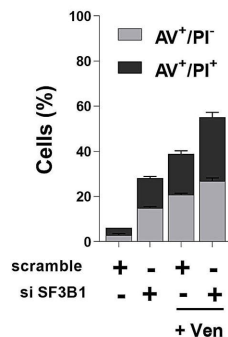
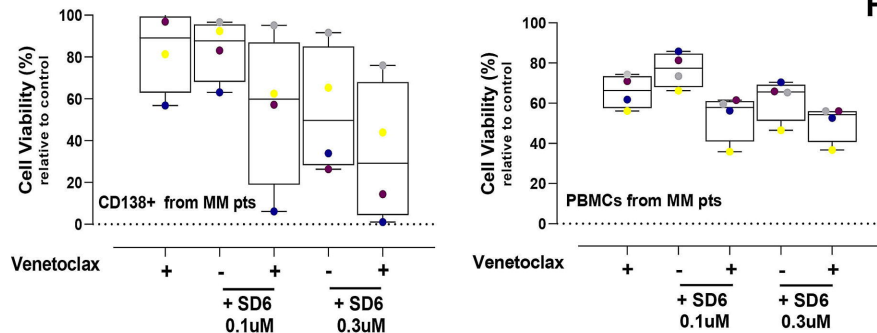
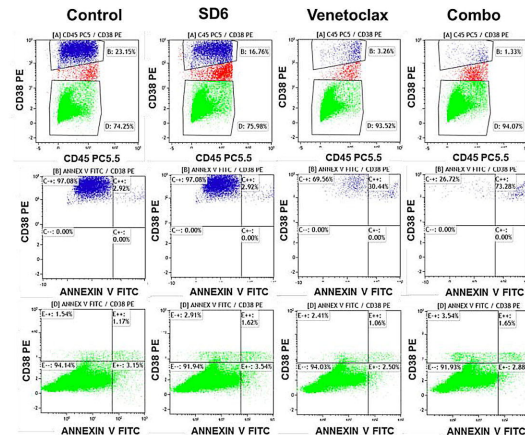
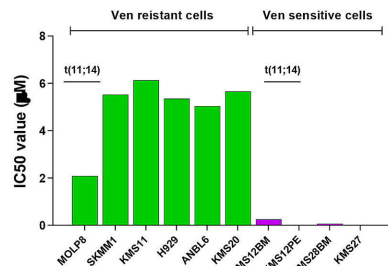
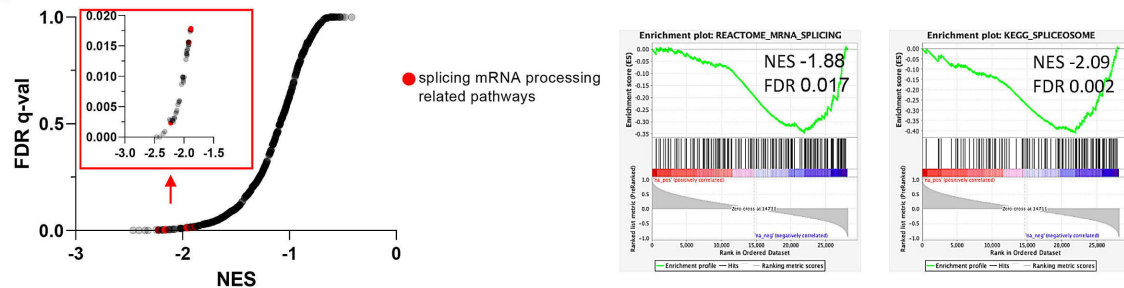
A) MM1S cells (4.5×10^6 cells/mouse) were implanted in both flanks of female NOD/SCID J mice (8 weeks of age). Tumor-bearing mice were randomized and treated with vehicle (n=10); Venetoclax (100 mg/kg; n=10) administered by oral gavage once a day for 15 days; SD6 (12 mg/kg; n=10) intratumorally once a day for 10 days and their combination (n=10). A significant delay in tumor growth in combination-treated mice was noted compared to vehicle-treated control mice (*** $p \leq 0.001$). Data are mean tumor volume \pm s.e.m. **B)** At the end of the experiment, mice were sacrificed, and tumor masses were imaged and weighed. (n.s. not significant, * $p \leq 0.05$, ** $p \leq 0.01$). **C)** Kaplan-Meier analysis showing significant survival benefit for mice treated with the combo, compared with single-agent treatment SD6 ($p = 0.0169$, Log-rank (Mantel-Cox) Test). **D)** Histogram pots show caspase 3 positive cells and mitosis observed in 10 observations in tumors harvested from mice treated with indicated stimuli. (* $p \leq 0.05$, ** $p \leq 0.01$). **E)** Immunohistochemical analysis for hematoxylin and eosin (H&E) and cleaved caspase 3 in xenografts tumors harvested from mice treated with control, SD6, Venetoclax or co-treatment. Tumor sections from treated and untreated mice stained with H&E were also analyzed for apoptotic bodies formation by using higher magnification. Red arrows indicate apoptotic bodies in each panel. Scale bar, 50 μ m **F)** MM1S xenograft-bearing, 8-week-old female NOD/SCID J mice were treated with vehicle (n=6); E7107 (2.5 mg/kg; n=9) intravenous once a day for 5 days; Venetoclax (100 mg/kg; n=8) oral administration once a day for 5 days and their combination (n=11). A significant delay in tumor growth in co-treated mice was noted compared to E7107-treated control mice (* $p = 0.0455$). Bars indicate mean \pm s.e.m. **G)** Kaplan-Meier survival plot showing significant increase in

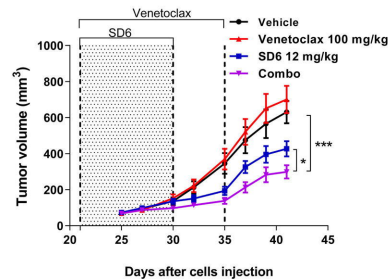
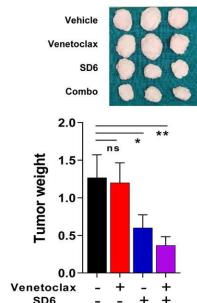
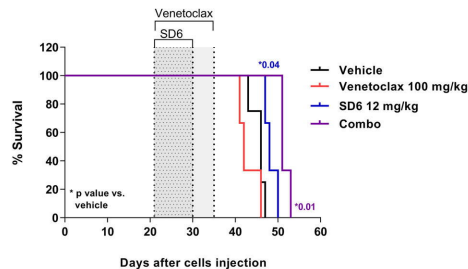
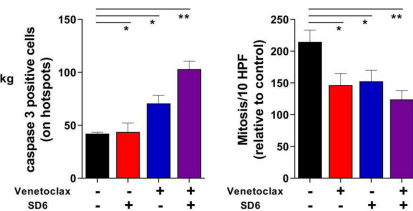
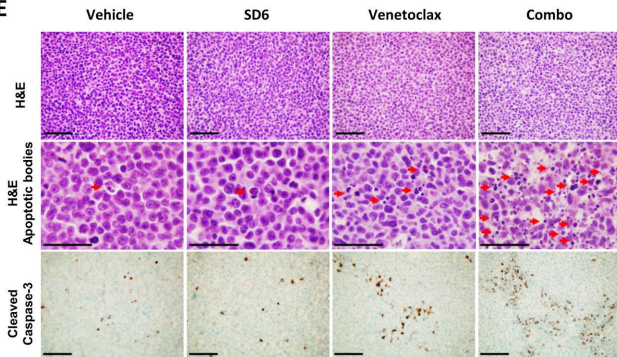
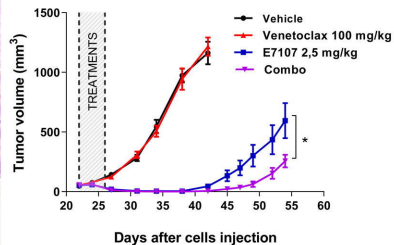
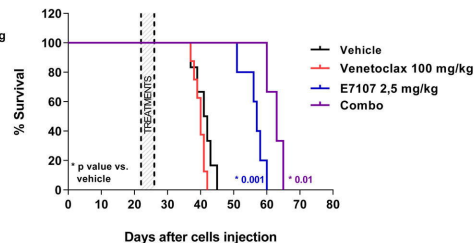
survival of mice receiving the combination of E7107 plus Venetoclax compared to E7107 single agent treated mice (combo vs E7107 $p=0.0295$). n indicates the number of tumors per treatment group. Data were analyzed by two-tailed Student's t-test (A, B, D, F) or by Log-rank (Mantel-Cox; C, F).

A**B****C****D****E****F**

A**B****C****D****E****F****G**

A**B****C****D****E****G****F****H**

A**B****C****D****E****F****G****H**

A**B****C****D****E****F****G**

Supplementary Data

Reagents

Meayamicin B and Sudemycin D6 (SD6) were kindly gifts from Prof. Kazunori Koide (University of Pittsburgh) and Prof. Thomas Webb (SRI Biosciences, Dept. of Chemistry and Biochemistry UCSC), respectively. E7107 was kindly provided by H3 Biomedicine, Inc.

Cell lines and culture

The HMCL were purchased from ATCC or DSMZ. All cell lines were Mycoplasma-free and routinely tested for it. Cells were cultured in RPMI-1640 medium containing 10% fetal bovine serum (FBS; GIBCO), 4mM glutamine, 100 U ml⁻¹ penicillin, and 100 µg ml⁻¹ streptomycin (GIBCO). 293T were cultured in DMEM high glucose containing 10% FBS (GIBCO), 4 mM glutamine, 100 U ml⁻¹ penicillin, and 100 µg ml⁻¹ streptomycin (GIBCO).

Primary cells

Peripheral blood samples collected from healthy volunteers were processed by Ficoll-Paque (GE Healthcare) gradient to obtain PBMCs. Malignant cells from individuals affected by MM were purified from bone marrow samples after informed consent was obtained in accordance with the Declaration of Helsinki and approval by the Ethical Committee at San Martino Policlinico in Genoa. Mononuclear cells were separated using Ficoll–Paque density sedimentation, and plasma cells were purified by positive selection (>95% CD138+) with anti–CD138 magnetic activated cell separation microbeads system (Miltenyi). Clinical and cytogenetic features of MM patients samples used for the study are shown in **Table S2**.

Lentiviral mediated gene transfer

pLV[shRNA]-EGFP:T2A:Puro-U6>Scramble_shRNA (shSCR) and pLV[shRNA]-EGFP:T2A:Puro-U6>hSF3B1[shRNA#1-4] (SF3B1 silencing plasmids), pLV[Exp]-CMV>EGFP:T2A:Puro (pLV empty vector) and pLV[Exp]-EGFP:T2A:Puro-SV40> hMYC (cMyc overexpressing plasmid) were used to create stable isogenic MM cell lines. pLV-EGFP/Neo-

SV40>Nluc was used to generate a stably expressing-NanoLuciferase MM cell line. All lentiviral plasmids were purchased from Vector Builder.

Tumor cell-specific bioluminescence imaging in co-cultures with stromal cells

7×10^3 Luciferase⁺ MM cells (H929 pLV-SV40-EGFP/Luc+) were plated in 96-well optical white plates in the presence or absence of pre-plated luciferase-negative primary stromal cells (20×10^3 cells seeded 24 hours before) and treated with drugs or vehicle (DMSO), as indicated. After 48 h of treatment, MM cell specific viability was assessed with Nano-Glo® Live Cell Assay System (Promega, #N2011) according to manufacturer's instructions.

Western blotting

Whole-cell lysates, SDS-page electrophoretic separation and blotting were performed as previously described¹. Primary antibodies used are detailed in Supplementary material (**Table S3**). Signals were acquired by I bright™ 1500 Imaging System using standard ECL (Thermo Fisher).

Immunofluorescence staining

DNA damage and nuclear speckles were detected by confocal microscopy, as described previously². The anti- γ H2AX antibody and the anti-SC35 antibody [SC-35]-Nuclear Speckle Marker were purchased from Millipore (Ser139, #05-636) and Abcam (#ab11826), respectively. The secondary Alexa Fluor 488-conjugated antibody was from Jackson ImmunoResearch (#115-546-006). γ H2AX foci and SC35 staining intensity were calculated by ImageJ-Find Maxima.

Cell Viability and Apoptosis Assay

MM cell lines viability and apoptosis were assessed as previously described². For MM primary cells, 3.5×10^3 CD138⁺ cells primary tumor cells were plated in white opaque 96-well plate in DMEM high glucose complete medium supplemented with IL-6 4 ng/ml. Then, cells were treated with drugs and 48 h later, cell viability was measured with CTG luminescent assay (Promega, #G7570) following manufacturer's instructions. For FACS analysis, 1×10^6 Bone Marrow-derived mononuclear cells from MM patients were treated with vehicle or drugs for 24 or 48 hours. After that, cells were stained with anti CD45-PC.5 (Beckman Coulter #A62835), anti CD38-PE (Becton

Dickinson #345806) and Annexin V-FITC (Miltenyi #130-093-060) and specific viability of CD38⁺ CD45⁻ or CD38⁻/ CD45⁻ gated MM cells was evaluated.

Transient transfection of MM cells

RPMI 8226 and AMO-1 SF3B1-silenced cells were generated by transient transfection of siRNAs (ON-TARGET plus SMART pool siRNA # L-020061-01-0005) using nucleofection. For each nucleofection, 2 x 10⁶ cells were pulsed with the DN-100 and DA-100 program respectively, using Amaxa SF Cell line 4-D Nucleofector X KitL (Lonza). siRNAs were used at the final concentration of 500 nM. After 24h from nucleofection, cells were treated and used for further experiments.

RT-PCR and Quantitative Real-time PCR (qPCR)

Total RNA was extracted from cells using the RNeasy mini kit (Qiagen, #74134d) according to the manufacturer's instructions. 1 µg of RNA was reverse-transcribed in a final volume of 50 µl using High Capacity cDNA Reverse Transcription kit (Applied Biosystem, #4368814). For validation of splicing inhibitors targets, a 35-cycle PCR was performed (1 minute of annealing at 60°C and a 2-minute extension at 72°C). All PCR products were separated and visualized on 2% agarose gels. For qPCR, 5 µl of the resulting cDNA was used for QPCR with a QuantStudio™ 5 Real-Time PCR System (Applied Biosystem, Thermo Scientific). mRNA levels were detected using SYBR Select Master Mix (Applied Biosystem, #4472918) according to manufacturer's protocol. Gene expression was normalized to housekeeping gene expression (β-actin). Comparisons in gene expression were calculated using the 2^{-ΔΔCt} method. PCR and quantitative PCR (qPCR) primers are listed in **Table S4**.

TaqMan Array Plates

Total RNA from previously isolated Peripheral Blood Mononuclear Cells (PBMCs) or CD138⁺ plasma cells was extracted using the RNeasy plus mini kit (Qiagen, #74134) according to the manufacturer's instructions and verified for quality with Nanodrop™ OneC (Thermo Scientific). 1µg of RNA was reverse-transcribed in a final volume of 20µl using SuperScript IV VILO Master Mix with ezDNase Enzyme (Applied Biosystem, #11766050) and diluted in 480µl of water to

obtain a final cDNA concentration of 10 ng per well. After that, 500µl of TaqMan Fast Advanced Master Mix (Applied Biosystem, # 4444963) were added to each sample and the mix was spotted on a 96-well 0.1µl Custom TaqMan Array plate (array ID: RPH49YH). Each plate contains 32 different TaqMan dried-down gene assays (including 3 housekeeping genes), in triplicate. QuantStudio™ 5 Real-Time PCR System (Applied Biosystem, Thermo Scientific) was employed. Results were analyzed with the $\Delta\Delta\text{Ct}$ method.³ Log2 transformed ΔCt were used to draw the heatmap in R with heatmap.2 function in the gplots package and the RColorBrewer package. Z-scores of the expression levels among rows were calculated and genes divided in high expression ($\text{Z-score} > 1$) and low expression ($\text{Z-score} < -1$). A list of genes included in the TaqMan Array plate is in **Table S5**.

Gene expression analysis of spliceosome signature in external MM datasets

Gene expression profiling data were derived from publicly available Gene Expression Omnibus (GEO) datasets profiled on Affymetrix Human Gene 1.0 ST array, available at accession numbers GSE66293 and GSE47552. Enrichment scores based on the expression levels of KEGG Spliceosome gene set (124 genes) from the Molecular Signatures Database (MSigDB) were calculated for microarray (GSE66293, GSE47552) and RNA-seq data (CoMMpass 774 MM dataset), respectively. As previously described¹, the gsva function in the Gene Set VariationAnalysis package for microarray and RNA-sequencing data (GSVA, version 3.8) was applied in R Bioconductor (version 4.0.2), by choosing the z-score method and Gaussian distribution. Samples were then stratified into low ($\text{z-score} \leq -1$), intermediate ($-1 < \text{z-score} < 1$), or high ($\text{z-score} \geq 1$) groups. The heatmap of KEGG Spliceosome signature was generated using DNA-Chip Analyzer software.⁴

Multi-Omics Data in CoMMpass Study

Multi-omics data about newly diagnosed bone marrow MM samples (BM_1) were freely available from Multiple Myeloma Research Foundation (MMRF) CoMMpass Study⁵ and obtained from the Interim Analysis 15a (MMRF_CoMMpass_IA15a). Transcript per Million (TPM) reads values

were obtained by Salmon gene expression quantification (Salmon_V7.2) for 774 BM_1 MM patients. Non-synonymous (NS) somatic mutation variants data were derived from whole exome sequencing (WES) analyses; copy number alteration (CNA) data were obtained by means of Next generation Sequencing (NGS)-based fluorescence in situ hybridization (FISH) analyses in the 414 MM cases classified in the two extreme quartiles and for which molecular data were available. The presence of a specific CNA was determined at a 20 percent cut-off, when occurring in at least one of the investigated cytoband (1q21, 13q14, 13q34 or RB1 locus).

Survival analyses in CoMMpass study

Kaplan-Meier analysis was applied on Overall Survival (OS) and Progression Free Survival (PFS) data in 299 and 343 MM patients, respectively stratified in low and high z-score groups. Log-Rank test was applied to measure the difference between survival curves.

Cox proportional hazards model was applied as univariate analysis on single molecular variables and International Staging System (ISS) groups in relation to OS and PFS data, in 414 MM cases, classified in low or high spliceosome group and for which all information were accessible.

Global analysis of alternative splicing patterns in CoMMpass study

The analysis of genome-wide patterns in alternative splicing was performed by means of IsoformSwitchAnalyzeR package in R Bioconductor (v4.0.2)⁶, by stratifying 774 MM samples of CoMMpass study according to SF3B1 expression level and comparing the extreme quartiles, each including 194 MM cases. Filtered Transcripts Per Million (TPM) and transcript counts obtained by RNA-sequencing (Salmon v7.2) and filtered GRCh37.74.gtf file from CoMMpass study were used to create isoform data matrices (194622 transcripts). After filtering out the isoforms not/low expressed in any samples, under stringent conditions (gene expression cut-off = 10, isoform expression cut-off = 3), isoforms switch analysis and prediction of alternative splicing was performed for 6388 gene comparisons by means of DRIMSeq.⁷ Significant splicing enrichment results were finally obtained in top compared to bottom SF3B1 quartile.

MM cell lines gene set enrichment analysis

For pathway enrichment analysis of Venetoclax resistant versus sensitive cell lines with published transcriptome data, activity areas were Pearson-correlated to the level of individual gene transcripts across cell lines. Gene-centric RMA-normalized mRNA expression data was acquired from CCLE.^{8,9} The resulting ranked Pearson-correlation-score / gene transcript matrix was then used as an input for the pre-ranked list tool of gene set enrichment analysis (GSEA).¹⁰ Enrichment scores were calculated for the following Molecular Signatures Database (MSigDB) collection CP:REACTOME: Reactome gene sets.¹¹ Significant pathways were selected based on FDR q-value <25%.

Highlighted REACTOME splicing / mRNA processing data sets: SNRNP_ASSEMBLY, PROCESSING_OF_CAPPED_INTRON_CONTAINING_PRE_MRNA, REACTOME_MRNA_SPLICING, REACTOME_MRNA_SPLICING_MINOR_PATHWAY. Enrichment plots were generated with GSEA software for REACTOME_MRNA_SPLICING and KEGG_SPLICEOSOME gene sets.

In situ detection of apoptosis and proliferation

Mice tumor sections were subjected to immunohistochemical staining for caspase-3 activation to detect apoptotic cell death. Visualization of apoptotic cells was done under a light microscope at ×40 magnification and was identified based on morphological features as described.¹² Tumor sections from treated and untreated mice stained with H&E and evaluated under light microscopy. Apoptotic cells were counted in 10 random fields. In each section, 1000 cells were evaluated for the presence of apoptotic cells and calculated as the number of apoptotic cells expressed as a percentage of the total number of non-apoptotic cells counted in each case.

Statistical analyses

All in vitro experiments were repeated at least three times and performed in triplicate; representative experiments are shown in figures. All data are shown as mean ± standard deviation (SD). The Student's t test was used to compare two experimental groups using Graph-Pad Prism software 8.4.3 (<http://www.graphpad.com>). The minimal level of significance was specified as

$p < 0.05$. Tumor volume was analyzed by two-way Student's t-test and data are shown as mean \pm s.e.m. Survival in *in vivo* experiments was evaluated by Log-rank (Mantel-Cox) Test. Drug interaction were assessed by CalcuSyn 2.0 software (Biosoft), which is based on the Chou-Talalay method. Combination Index (CI) = 1, indicates additive effect; CI < 1 indicates synergism; CI > 1 indicates antagonism.

TABLEs for supplementary data

Table S1. IC50 values for indicated spliceosome modulators

HMCLs	MeaymicinB IC50 (nM)	Sudamicin D6 IC50 (nM)	E7107 (nM)
KMS34	0.53	Not tested	Not tested
KMS20	1.03	Not tested	Not tested
LP1	2.66	Not tested	Not tested
MM1S	0.80	472.8	1.1
KMS11	1.16	Not tested	Not tested
U266	0.50	588.6	Not tested
MOLP8	0.51	Not tested	Not tested
AMO1	1.71	32.25	Not tested
KMS12PE	0.49	Not tested	Not tested
H929	1.01	165.8	0.57
MR20	3.5	Not tested	Not tested
OPM2	0.96	Not tested	Not tested
LR5	2.24	Not tested	Not tested
RPMI8226	2.01	2789	Not tested

HMCLs: human multiple myeloma cell lines

Table S2. Clinical and cytogenetic features of MM patients

PATIENTS	AGE	SEX	ISOTYPE	R-ISS	DISEASE STATUS	FISH	PREVIOUS THERAPIES
MM#1	82	M	IgG _k	II	RRMM	SD	Bz
MM#2	66	F	IgAk	III	NDMM	del17p	None
MM#3	74	F	IgG λ	II	NDMM	SD	None
MM#4	74	F	IgG _k	II	NDMM	1q amp	None
MM#5	78	F	micromolecular	III	RRMM	t(4;14)	Bz/Len
MM#6	75	F	IgG λ	III	NDMM	t(14;16)	None
MM#7	74	M	IgG _k	II	RRMM	SD	Bz
MM#8	70	M	IgG _k	III	NDMM	del17p	None
MM#9	72	F	micromolecular	II	RRMM	SD	Bz/Len
MM#10	80	M	IgG λ	III	RRMM	t(4;14)	Len
MM#11	78	M	micromolecular	II	NDMM	SD	None
MM#12	80	M	IgG _k	III	RRMM	del17p	Bz/Len
MM#13	75	M	IgG _k	I	RRMM	SD	Bz
MM#14	71	M	IgG _k	II	RRMM	t(11,14)	Bz
MM#15	80	F	IgG _k	II	RRMM	SD	Bz
MM#16	77	M	IgG _k	II	RRMM	SD	Bz/Len/Dara
MM#17	67	M	IgG _k	II	NDMM	SD	None
MM#18	65	M	IgG _k	III	NDMM	del17p	None
MM#19	60	F	IgG _k	III	NDMM	del17p	None

MM#20	62	F	IgG λ	II	RRMM	SD	None
MM#21	72	F	IgA λ	III	RRMM	1q amp	Len
MM#22	67	M	IgA λ	III	RRMM	del 17p	Bz/Len
MM#23	75	F	IgG λ	II	NDMM	t(11;14)	None
MM#24	63	M	IgA κ	I	NDMM	SD	None
MM#25	82	M	IgG λ	II	RRMM	SD	Bz/Len
MM#26	73	M	IgG κ	III	RRMM	del17p	Bz
MM#27	79	M	IgG κ	I	NDMM	SD	None
MM#28	79	M	IgA λ	II	NDMM	SD	None

NDMM Newly diagnosed; RRMM resistant/refractory; SD standard risk, Bz: bortezomib; Len: lenalidomide; Dara: daratumumab

Table S3. Antibodies

mAb	Source	Product Number
Bcl-2	Cell Signalling Technology	4223
Bcl-xL	Cell Signalling Technology	2764
Mcl-1	Cell Signalling Technology	5453
SF3B1	Cell Signalling Technology	14434
phospho-SF3B1	Cell Signalling Technology	25009
PARP-1	Cell Signalling Technology	9542
Caspase3	Cell Signalling Technology	9662
cleaved-Caspase3	Cell Signalling Technology	9664
RAD51	SantaCruz Biotechnology	sc-8349
cMyc	Cell Signalling Technology	9402
γ H2AX	Cell Signalling Technology	05-636
gamma-Tubulin	Thermo Scientific	MA1-850
GAPDH	Cell Signalling Technology	5174

Table S4. PCR and quantitative PCR (qPCR) primers

Gene name	primer FORWARD 5'-3'	primer REVERSE 5'-3'
MCL1	GAGGAGGAGGAGGACGAGTT	ACCAGCTCCTACTCCAGCAA
BCL2	ATGTGTGTGGAGAGCGTCAA	CACTTGTGGCCCAGATAGG
BCLXL	GGGCATTCACTGACCTGACA	GGGAGGGTAGAGTGGATGGT
GAPDH	TCTCCTCTGACTTCAACAGCGAC	CCCTGTTGCTGTAGCCAAATTC
Delta2 MCL1	GCCAAGGACACAAAGCCAAT	AGTTTCCGAAGCATGCCTTG
Full length MCL1	GCCAAGGACACAAAGCCAAT	ACTCCACAAACCCATCCTTG

Table S5. Genes included in TaqMan Array plates

Genes included in Custom TaqMan Array plates			
18s rRNA	HNRNPA2B1	SF1	SNRPE
CLK1	HNRNPC	SF3A1	SNRPF
COIL	HNRNPD	SF3B1	SRSF1
GAPDH	HNRNPK	SF3B2	SRSF2
GEMIN2	HPRT1	SF3B6	STRAP
GEMIN6	PHF5A	SNRPD1	U2AF2
GEMIN7	PRMT5	SNRPD2	WDR77
HNRNPA1	PRPF8	SNRPD3	ZRSR2

REFERENCES

1. Soncini D, Minetto P, Martinuzzi C, et al. Amino acid depletion triggered by L-asparaginase sensitizes MM cells to carfilzomib by inducing mitochondria ROS-mediated cell death. *Blood Adv.* 2020;4(18):4312–4326.
2. Soncini D, Orecchioni S, Ruberti S, et al. The new small tyrosine-kinase inhibitor ARQ531 targets acute myeloid leukemia cells by disrupting multiple tumor-addicted programs. *Haematologica.* 2019;haematol.2019.224956.
3. Livak KJ, Schmittgen TD. Analysis of relative gene expression data using real-time quantitative PCR and the 2- $\Delta\Delta$ CT method. *Methods.* 2001;25(4):402–408.
4. Schadt EE, Li C, Ellis B, Wong WH. Feature extraction and normalization algorithms for high-density oligonucleotide gene expression array data. *J. Cell. Biochem. Suppl.* 2001;Suppl 37(SUPPL. 37):120–5.
5. MMRF Researcher.
6. Vitting-Seerup K, Sandelin A. IsoformSwitchAnalyzeR: analysis of changes in genome-wide patterns of alternative splicing and its functional consequences. *Bioinformatics.* 2019;35(21):4469–4471.
7. Robinson MD, Nowicka M. DRIMSeq: A Dirichlet-multinomial framework for multivariate count outcomes in genomics. *F1000Research.* 2016;5:.
8. Barretina J, Caponigro G, Stransky N, et al. The Cancer Cell Line Encyclopedia enables predictive modelling of anticancer drug sensitivity. *Nature.* 2012;
9. Broad Institute Cancer Cell Line Encyclopedia (CCLE).
10. Subramanian A, Tamayo P, Mootha VK, et al. Gene set enrichment analysis: A knowledge-based approach for interpreting genome-wide expression profiles. *Proc. Natl. Acad. Sci.* 2005;102(43):15545–15550.

11. Reactome Pathway Database.
12. Kerr JFR, Wyllie AH, Currie AR. Apoptosis: A basic biological phenomenon with wide-ranging implications in tissue kinetics. *Br. J. Cancer.* 1972;26(4):239–257.

Supplementary Figures and legends

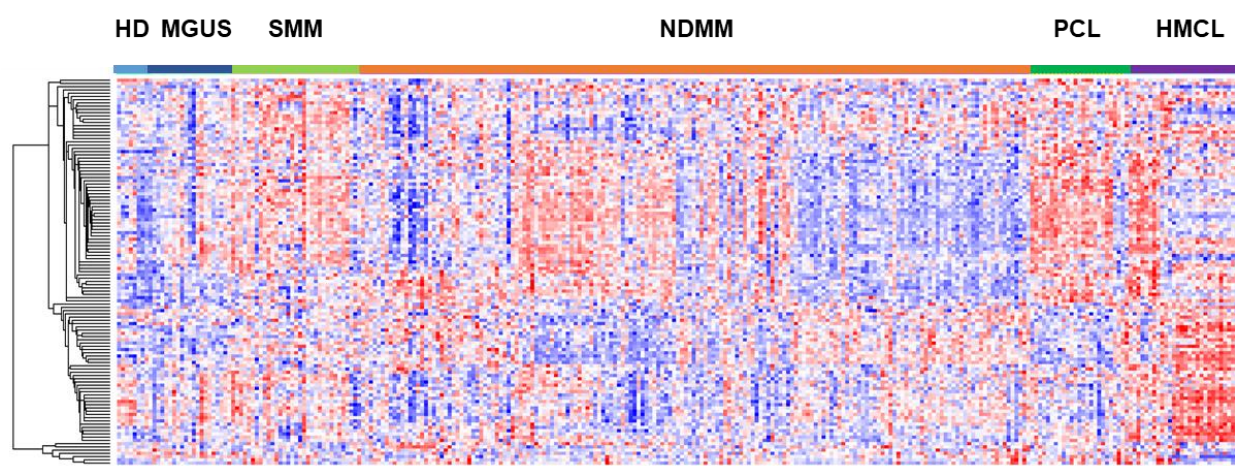


Figure S1. Heatmap showing expression levels for the genes corresponding to KEGG spliceosome gene set in plasma cells from healthy donors (normal, 9 N) or patients with monoclonal gammopathy of undetermined significance (20 MGUS), smoldering MM (33 SMM), active disease (170 MM), and secondary plasma cell leukemia (12 PCL) and in HMCLs (GSE66293 and GSE47552, profiled on Human Gene 1.0 ST Array). The color scale spans the relative gene expression changes standardized on the variance.

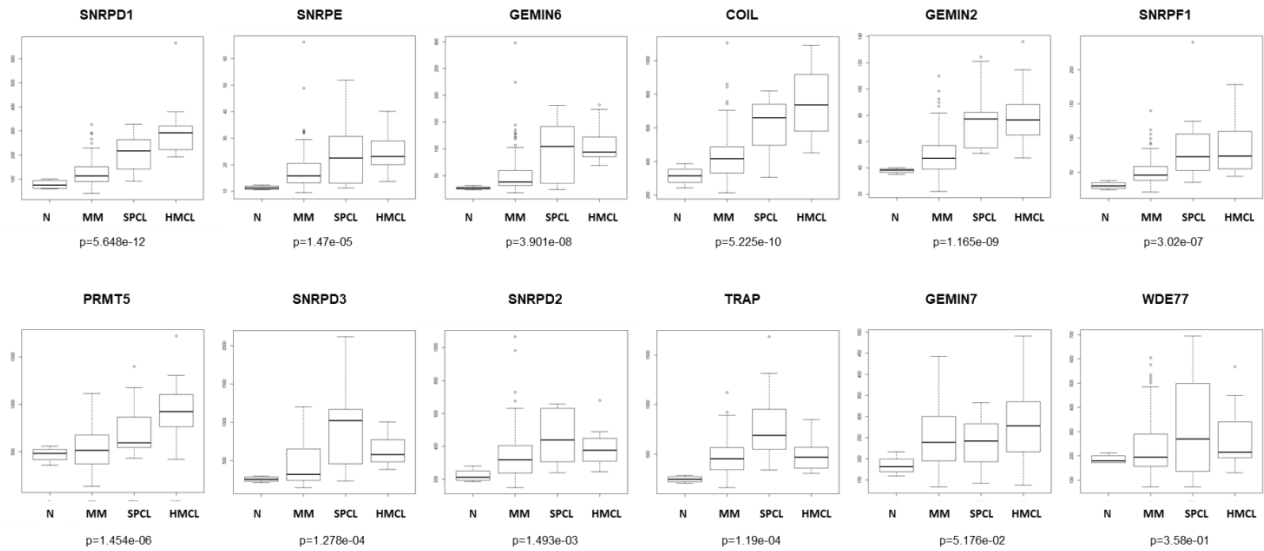


Figure S2. Box plot indicating the expression levels of SNRPD1, SNRPE, GEMIN6, COIL, GEMIN2, SNRPF1, PRMT5, SNRPD2, TRAP, GEMIN7 and WDE77 genes in a 323-sample dataset, including 4 healthy donors (N), 129 MM, 12SPCL patients, together with 18 HMCLs. This 323-sample dataset was generated using GSE66293. Global p-value (Kruskal-Wallis test) is indicated below.

Univariate Cox Regression analysis

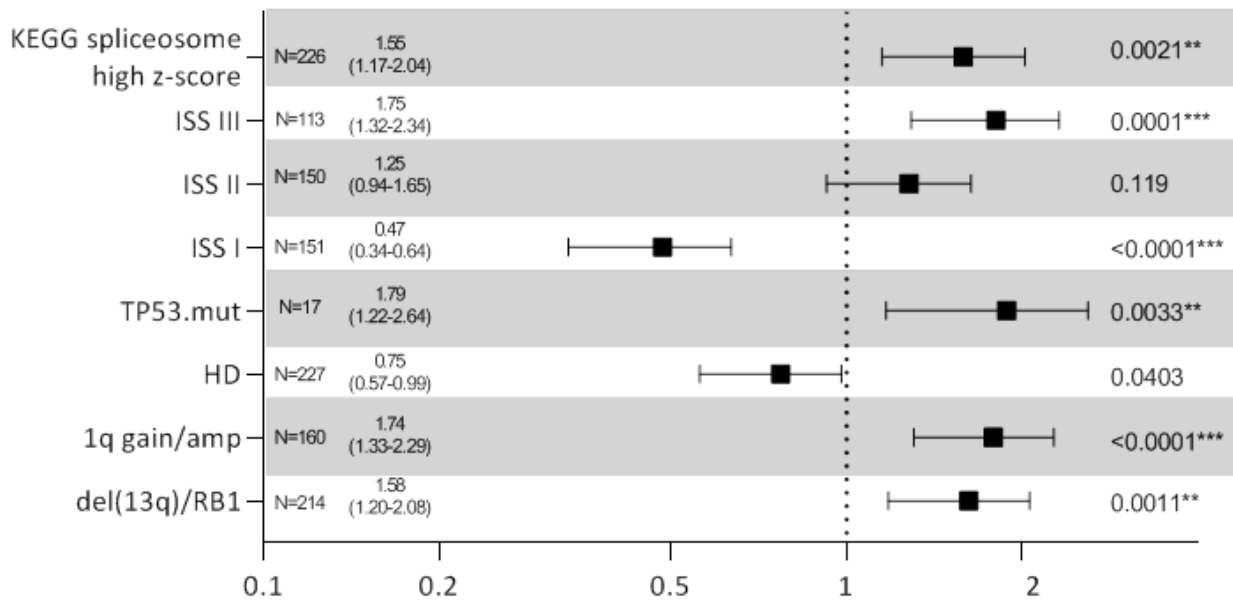


Figure S3. Forest plot based on Cox univariate analysis for progression free survival. Squares represent hazard ratios; bars represent 95% confidence intervals. p-values are reported on the right for each analysis.

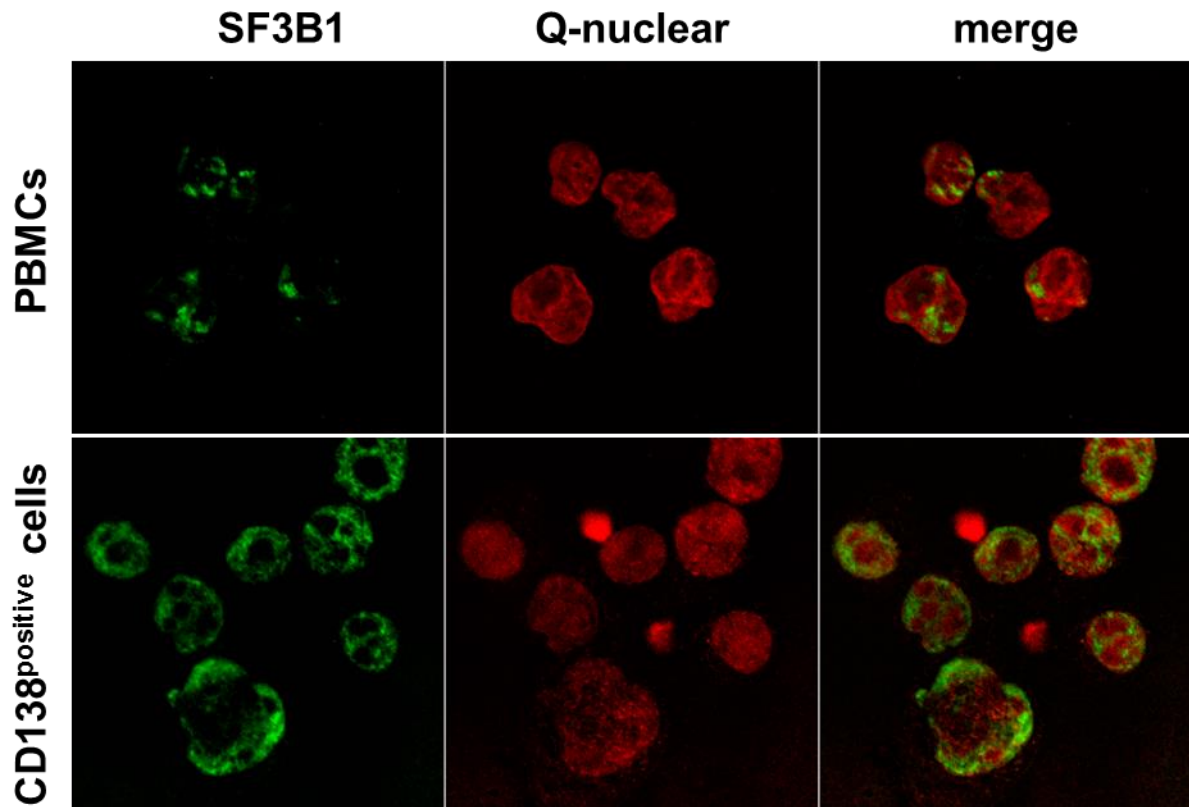


Figure S4. Detection of SF3B1 and Q-nuclear was measured by confocal microscopy in PBMCs (upper part) or MM tumor cells (bottom part) collected from a representative HD (healthy donor) and a MM patient, respectively.

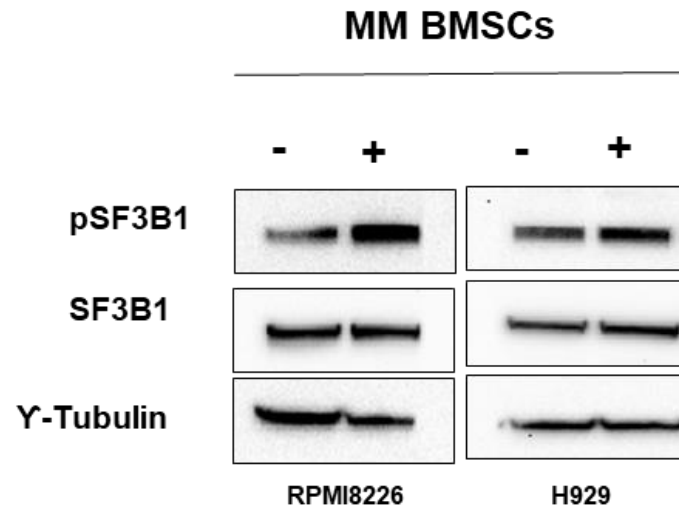


Figure S5. Western blot analysis of phopfo-SF3B1 and SF3B1 protein expression in indicated MM cells alone and after 48 hours of co-incubation with MM-patient derived BMSCs. Gamma tubulin was used as a loading control.

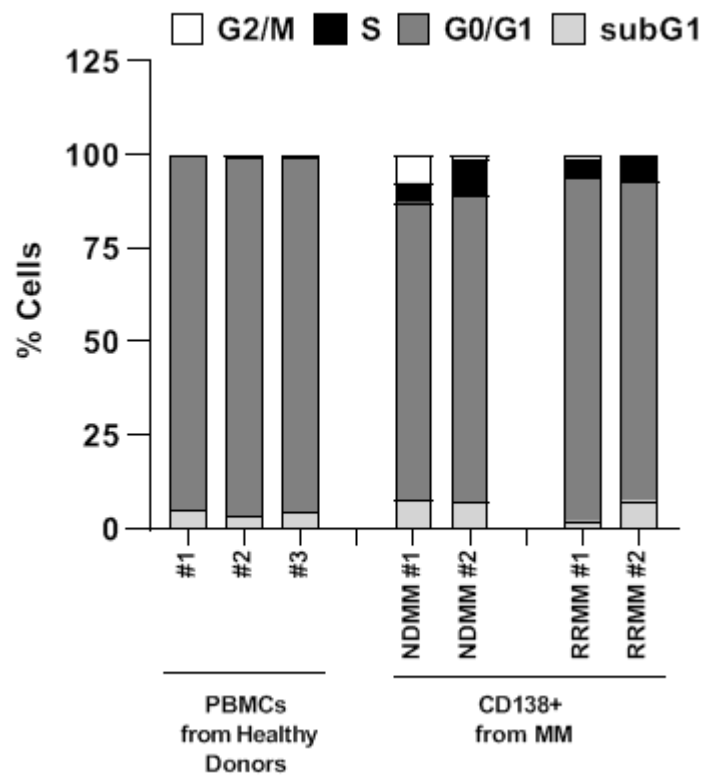


Figure S6. Cytofluorimetric analysis of cell cycle distributions of normal PBMCs cells and MM cells collected at indicated stage disease.

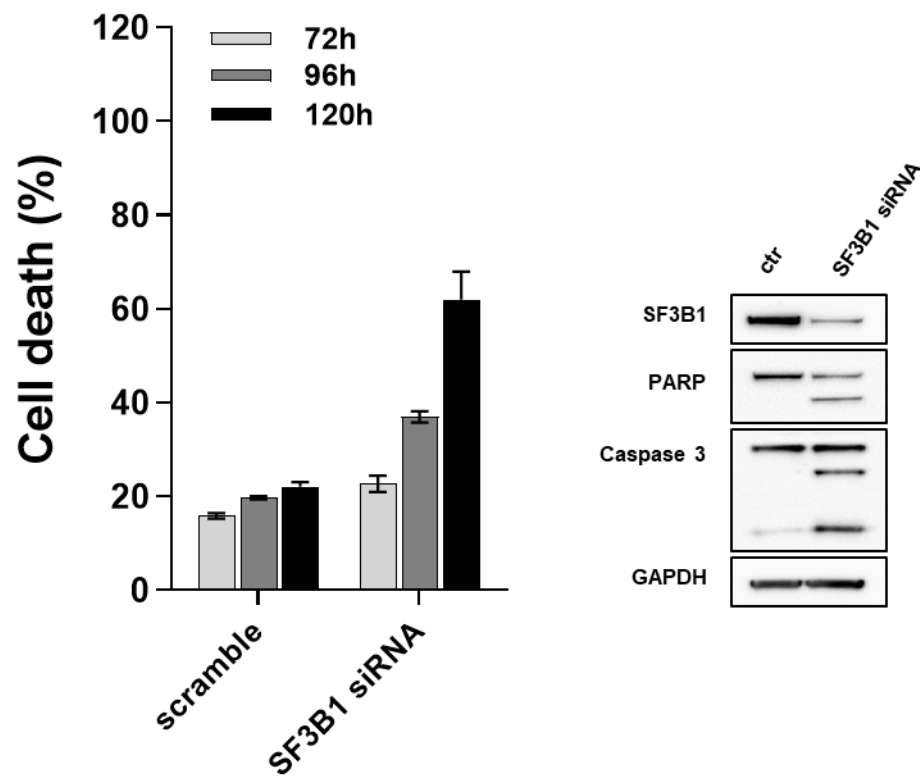


Figure S7. Cell death (measured with MTS assay) of SF3B1-silenced (nucleofected with specific siRNAs) or control (scramble siRNA) RPMI 8226 cells at indicated time points. On the right, western blot analysis of apoptotic markers (PARP1 and Caspase 3 cleavage) after 72hours from nucleofection. Data are representative of at least three independent experiments.

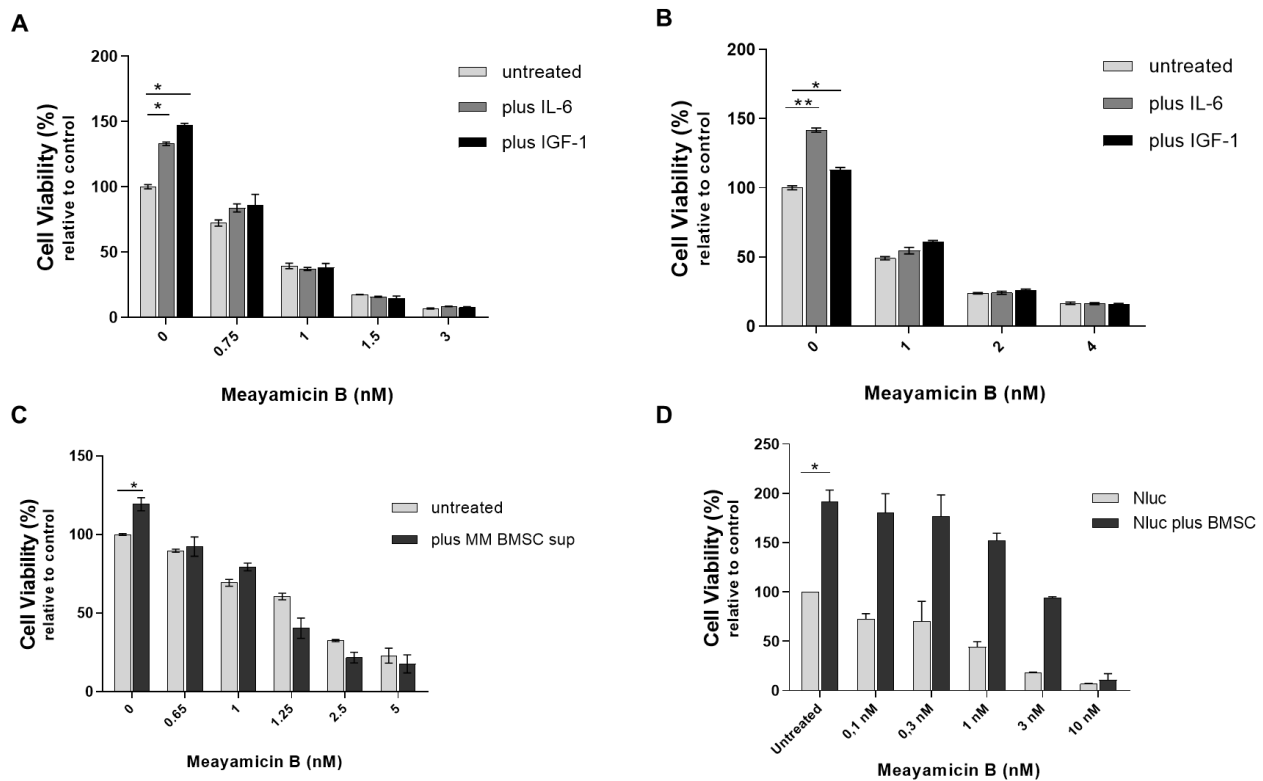


Figure S8. H929 (A) or MM1S (B) cells were treated with different doses of Meayamicin B for 48hours, (0.75-3nM) in presence or absence of rhIL-6 (10 ng/mL) or rhIGF-1 (100 ng/mL) for 48 hours, and viability was then measured by MTS assay. C) Viability of H929 cells treated with increasing doses of Meayamicin B for 48 hours, in presence or absence of BMSC-conditioned medium. Viability was then measured by MTS assay. D) Viability of H929 Nano Luc+ cells treated with increasing doses of Meayamicin B for 48 hours, alone and in the presence of MM patient–derived BMSCs (grey), measured by luciferase-based luminescence assay. The results presented in all panels are a mean \pm SD of triplicate samples (*P \leq 0.05; **P \leq 0.01; unpaired t test).

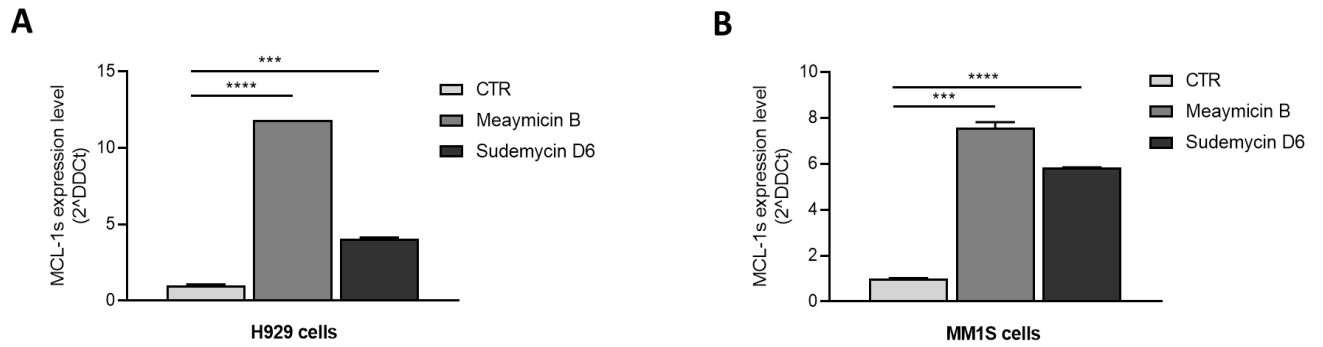


Figure S9. A-B) qPCR analysis for the pro-apoptotic short-form of MCL-1 (exon 2-skipped, MCL-1s) in H929 (**A**) or MM1S (**B**) cells treated for 6 hours with Meaymicin B (3 nM) or Sudemycin D6 (500 nM for H929 and 1.5 μ M for MM1S). GAPDH was used as housekeeping gene and $2^{-\Delta\Delta C_t}$ method was used for the analysis. Results are a mean \pm SD of triplicate samples (*** $P \leq 0.001$; **** $P \leq 0.0001$).

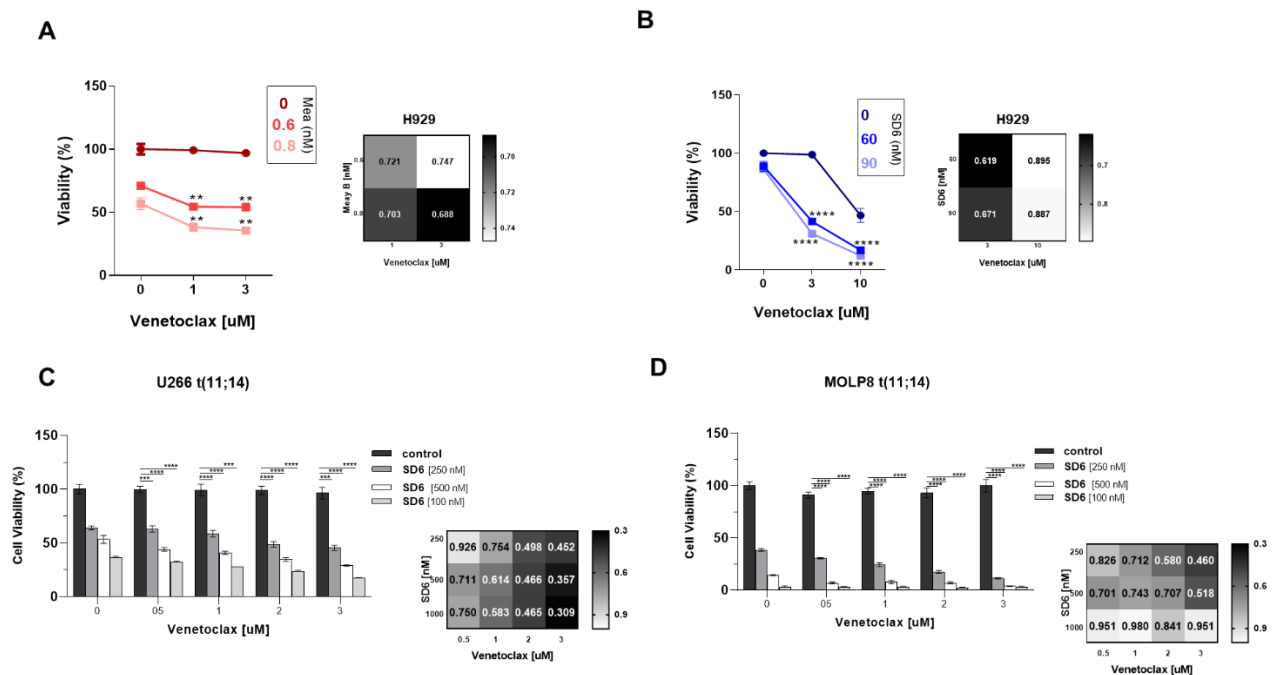


Figure S10. A-B) Cell viability curves of H929 combination therapy with MeaymcinB (left) or Sudemycin D6 (right) and Venetoclax. **C-D)** Cell viability curves of indicated t(11;14) MM cell lines following combination therapy with Sudemycin D6 and Venetoclax. CI synergy score (calculated with CalcuSyn software) for each set of drugs combination is indicated. Data are presented as mean \pm S.D (n=3). (***) $p \leq 0.01$, (****) $p \leq 0.001$; unpaired t test).

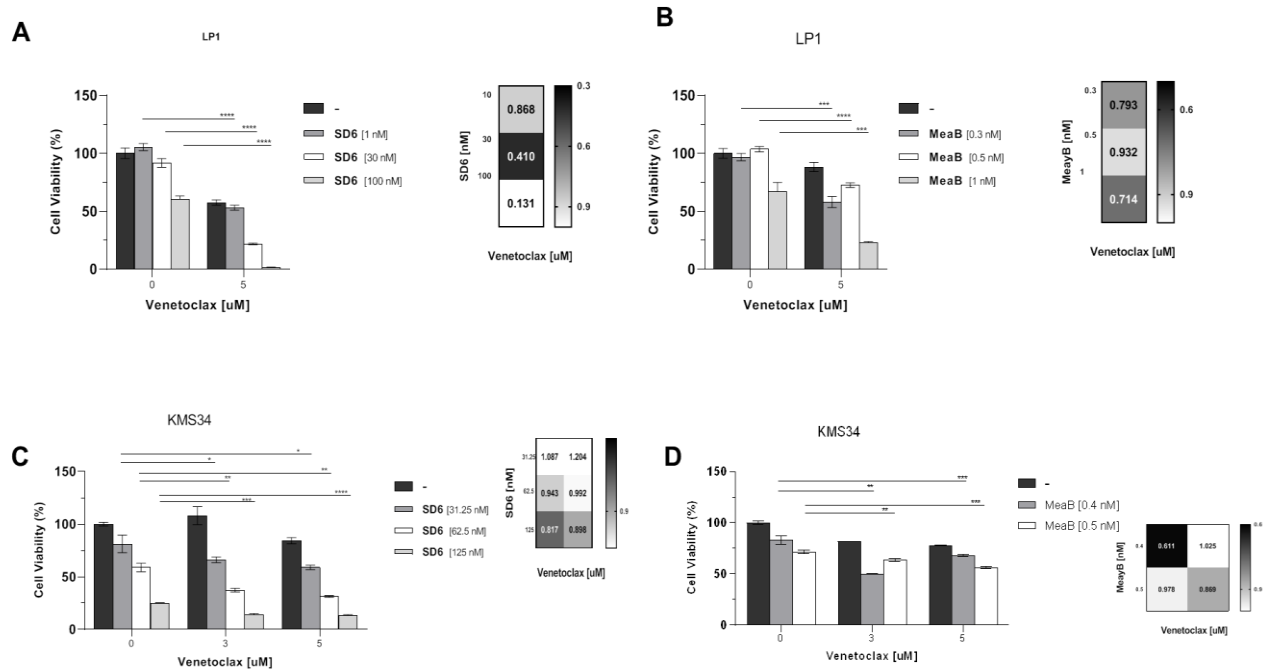


Figure S11. Cell viability curves of LP1 and KMS34 combination therapy with Sudemycin D6 (upper) or MeaymcinB (bottom) and Venetoclax. CI synergy score (calculated with CalcuSyn software) for each set of drugs combination is indicated. Data are presented as mean \pm S.D (n=3). (***) $p \leq 0.01$, (****) $p \leq 0.001$; unpaired t test).

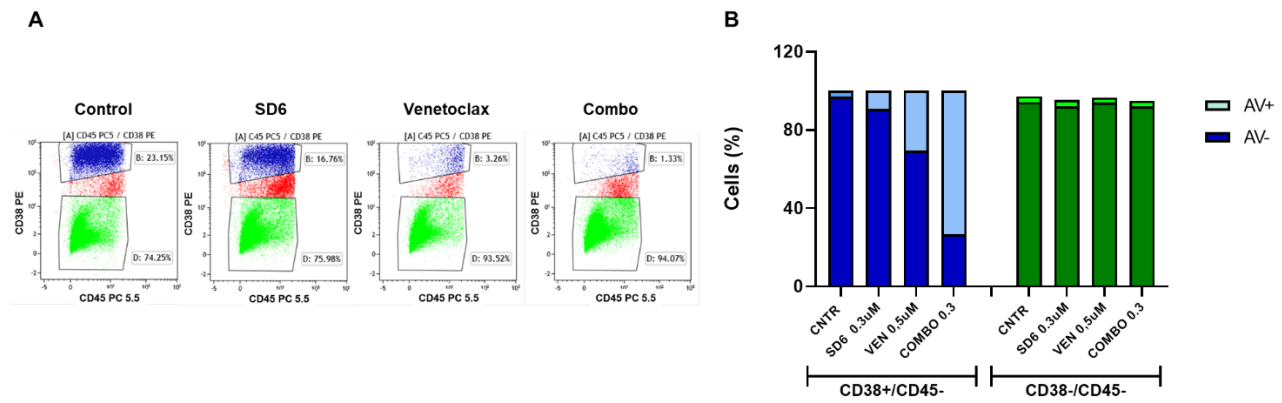


Figure S12. **A)** Flow plots of one representative MM patient sample (MM17). MM ($CD38^+ CD45^-$) and BMSCs-gated cells ($CD38^- CD45^-$) were quantified. **B)** Histograms showing percentages of Annexin V positive and negative cells in each gated population after 48hours of drugs exposure.

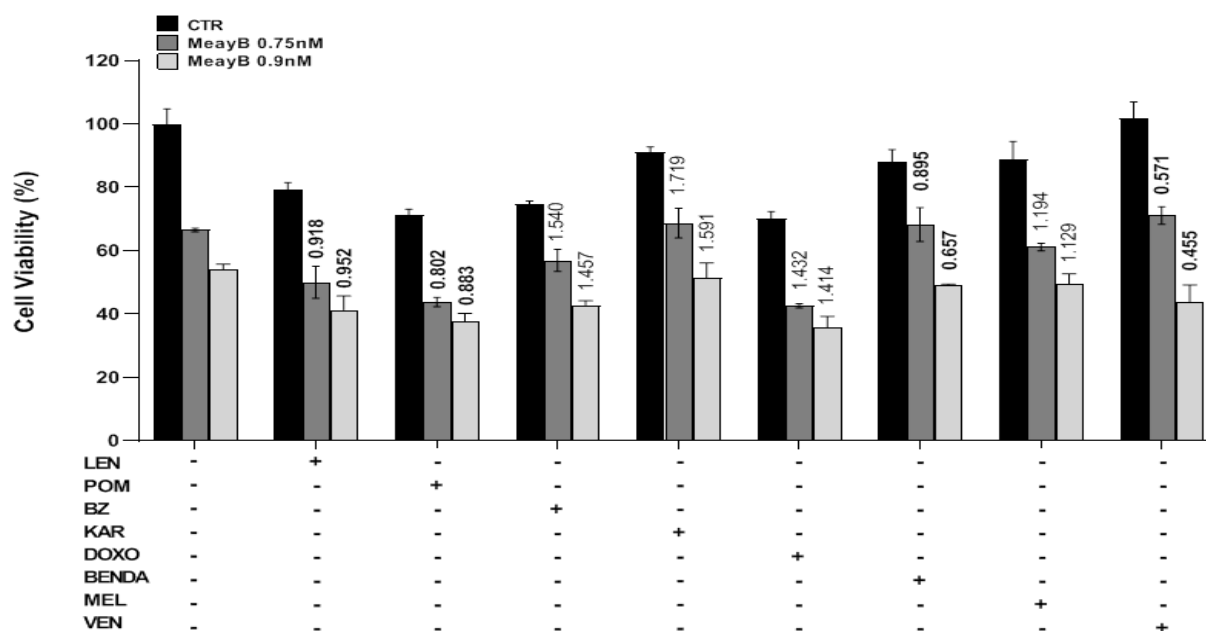


Figure S13. NCI-H929 cells were incubated in 96-well plates in the presence or absence of 0.75 or 0.9 nM MeaymicinB and different anti-MM drugs (2.5 μ M Lenalidomide, 0.25 μ M Pomalidomide, 3 nM Bortezomib, 2 nM Carfilzomib, 60 nM Doxorubicin, 30 μ M Bendamustine, 1 μ M Melphalan, and 3 μ M Venetoclax) or their combination. Cell death was assessed 48 hours later by MTS-viability assay. Results are means of triplicates \pm SD; CI synergy score (calculated with CalcuSyn software) for each set of drugs combination is also indicated.

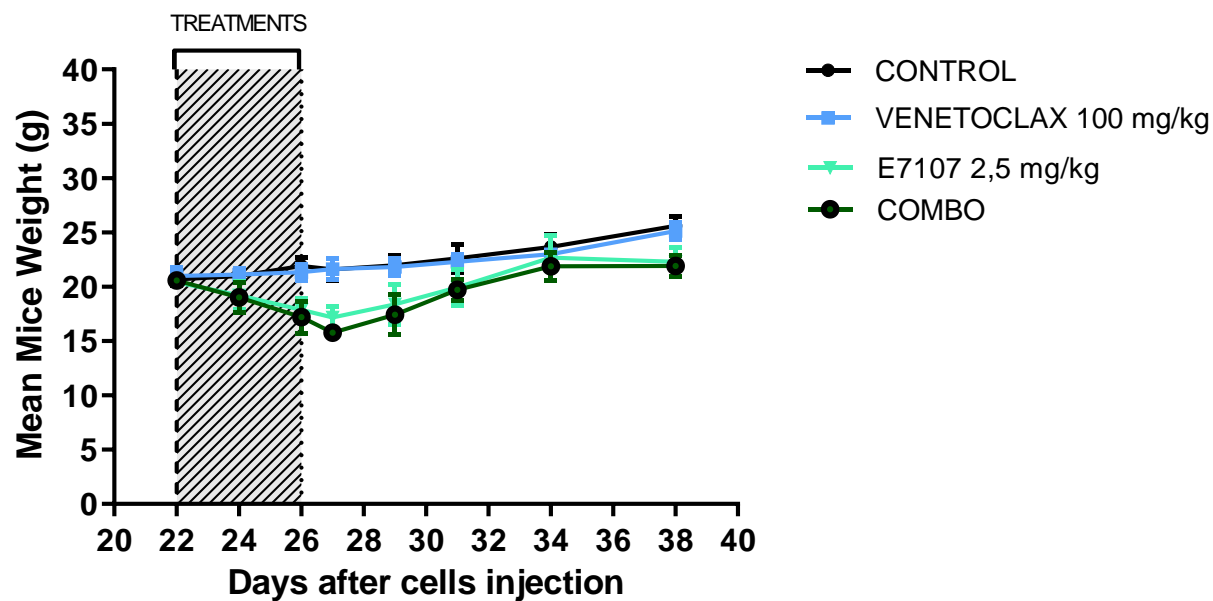


Figure S14. Mean mice weight \pm SD for each treated group over time. Days after MM cell injection and treatment schedule are indicated as well.